Redox Biology 86 (2025) 103794

Contents lists available at ScienceDirect

Redox Biology

journal homepage: www.elsevier.com/locate/redox

Functional analysis of bipartite NRF2 activators that overcome feedback regulation for age-related chronic diseases

Dmitry M. Hushpulian [a,1], Navneet Ammal Kaidery [b,c,1], Priyanka Soni [b,c], Andrey A. Poloznikov [d], Arpenik A. Zakhariants [e], Alexandra V. Razumovskaya [f], Mariia O. Silkina [f], Vladimir I. Tishkov [g], Eliot H. Kazakov [h], Abraham M. Brown [h], Irina N. Gaisina [i], Young-Hoon Ahn [j], Sergey V. Kazakov [k], Nancy Krucher [k], Sudarshana M. Sharma [l,m], Bindu D. Paul [n,o,p], Irina G. Gazaryan [k], Sergey V. Nikulin [f], Bobby Thomas [b,c,q,r,*]

[a] Laboratory of Molecular Engineering, Federal Research Center "Fundamentals of Biotechnology", Russian Academy of Sciences, Moscow, Russia
[b] Darby Children's Research Institute, USA
[c] Departments of Pediatrics, Medical University of South Carolina, Charleston, SC, USA
[d] SciBerg e.Kfm, James-Monroe-Ring 107, Mannheim, Germany
[e] Shemyakin-Ovchinnikov Institute of Bioorganic Chemistry, Russian Academy of Sciences, Moscow, Russia
[f] Faculty of Biology and Biotechnologies, HSE University, Moscow, Russia
[g] Department of Chemical Enzymology, Lomonosov Moscow State University, Moscow, Russia
[h] Department of Anatomy and Cell Biology, New York Medical College, Valhalla, NY, USA
[i] Department of Pharmaceutical Sciences and UICentre, Retzky College of Pharmacy, University of Illinois at Chicago, Chicago, IL, USA
[j] Department of Chemistry, College of Arts and Sciences, Drexel University, Philadelphia, PA, USA
[k] Dyson College of Arts and Sciences, Pace University, Pleasantville, NY, 10570, USA
[l] Department of Biochemistry and Molecular Biology, USA
[m] Hollings Cancer Center, Medical University of South Carolina, Charleston, SC, USA
[n] Departments of Pharmacology and Molecular Sciences, USA
[o] The Solomon H. Snyder Department of Neuroscience, USA
[p] Psychiatry and Behavioral Sciences, Johns Hopkins University School of Medicine, Baltimore, MD, USA
[q] Department of Neuroscience, USA
[r] Department of Drug Discovery, Medical University of South Carolina, Charleston, SC, USA

ARTICLE INFO

Keywords:
Cell-permeable Nrf2 peptide
Displacement activator
Luciferase fusion assay
Bach1 inhibitor
Keap1 protein quantification
Comparative transcriptomics

ABSTRACT

Activating Nrf2 with small molecules is a promising strategy for countering aging, oxidative stress, inflammation, and various disorders, including neurodegeneration. The primary regulator of Nrf2 protein stability is Keap1, a redox sensor protein and an adapter in the Cullin III ubiquitin ligase complex, which labels Nrf2 for proteasomal degradation. The canonical Nrf2 activators either chemically modify sensor thiols in Keap1 or competitively displace Nrf2 from the ubiquitin ligase complex. The latter approach is considered the most suitable for continuous administration, as non-specific chemical modifiers of Keap1 thiols also modify active thiols on other cellular proteins, causing side effects. However, when transitioning from homogeneous cell-free to cell-based assays, genuine displacement activators show a significant loss in potency by several orders of magnitude. We demonstrate that this discrepancy arises due to higher micromolar concentrations of Keap1 in cell lines. The absolute amounts of Nrf2 and Keap1 determined in brain sub-regions show more than an order of magnitude excess of Keap1 over Nrf2. A potential solution could involve targeted delivery of an alkylating agent to Keap1 to achieve the desired specificity. Transcriptomic analysis of a cell-permeable Nrf2 peptide bearing an alkylating fumarate moiety indicates selective activation of the Nrf2 genetic program, confirming the high specificity of this approach. Activation of the Nrf2-genetic program has a built-in feedback regulatory mechanism through Bach1, an Nrf2 transcriptional repressor, whose levels are elevated in age-related neurodegeneration. Thus, a benign

* Corresponding author. Departments of Pediatrics, Medical University of South Carolina, Charleston, SC, USA.
E-mail address: thomasbo@musc.edu (B. Thomas).
[1] These authors contributed equally.

https://doi.org/10.1016/j.redox.2025.103794
Received 1 July 2025; Received in revised form 19 July 2025; Accepted 28 July 2025
Available online 30 July 2025

bipartite Nrf2 activator with Bach1 inhibition properties is needed for maximal benefits. The recently developed heterocyclic carboxamide, HPPE, exhibits overlap with the Nrf2 pathway activated by the fumarate-linked Nrf2 peptide, an Nrf2 activator, as well as with zinc and tin protoporphyrins, which are inhibitors of Bach1. Therefore, HPPE presents a promising and unique combination of the two desired activities that could be further optimized to treat age-related neurodegeneration.

1. Introduction

Cellular redox homeostasis is regulated by the intrinsic genetic program, orchestrated by the key transcription factor nuclear factor erythroid 2-related factor 2 (Nrf2). Nrf2 is constitutively synthesized in the cell and in the absence of oxidative or xenobiotic stress, undergoes proteasomal degradation through its interaction with the adapter protein Kelch-like ECH-associated protein 1 (Keap1), a redox sensor in the ubiquitin ligase Cul III complex. Two other stress-induced mechanisms for fine-tuning Nrf2 protein stability occur via beta-transducin repeat-containing E3 ubiquitin-protein ligase (β-TrCP) and E3 ubiquitin-protein ligase synoviolin (Hrd1), which play a secondary role [1]. Keap1 has a set of highly reactive thiols, which, when modified, disrupt the Nrf2/Keap1 or Keap1/Cul III interactions, resulting in the stabilization of the Nrf2 protein. The Nrf2-mediated genetic program is subject to negative feedback regulation through the upregulation of both Keap1 [2] and the transcriptional repressor BTB and CNC homology 1 (Bach1) [3]. Maintaining proper Nrf2/Keap1 homeostasis is crucial for various cellular functions, including cellular repair and survival, detoxification, metabolism, autophagy, proteostasis, inflammation, and differentiation [4–6]. Nrf2 activation is also known to play a key role in reversing nuclear aging defects in premature aging and other age-related diseases [7]. Therefore, Nrf2 is a well-justified target for medical intervention to prevent and treat age-related diseases of various etiologies.

Multiple approaches have been followed to harness the Nrf2 pathway for therapeutic benefits. Activation of the Nrf2-driven genetic program with small molecules that modify thiols on Keap1 is a popular approach, despite the existence of unavoidable side effects originating from the non-specific thiol modification by canonical Nrf2 activators, including FDA-approved medications based on fumarate esters (Tecfidera, Vumerity, Bafiertam) [8]. Hence, the development of Nrf2 activators intended to treat ongoing neurodegeneration must take into consideration these aspects, as non-specific thiol modifications compromise the activity of numerous cellular defense proteins and enzymes, and increase the level of reactive oxygen species (ROS), which are already elevated in neurodegenerative states. One solution to the problem is the development of competitive and reversible Nrf2 displacement activators. However, the current generation of displacement activators with high Keap1 binding affinity fails to display a low EC_{50}, necessitating high doses of displacement activators for cell-based assays and *in vivo* applications. To gain a precise understanding of the problem of low effectiveness of Nrf2 displacement activators, we employed a range of novel small molecules and biologics, as well as various experimental methodologies, including a proprietary reporter assay, protein quantification, and transcriptomic approaches, to formulate the requirements for developing an ideal Nrf2 activator. Our findings lay the groundwork for developing novel therapeutics that target the Nrf2 signaling cascade in aging and neurodegenerative diseases, while minimizing side effects and enhancing therapeutic benefits.

2. Materials and methods

2.1. Animals

We used both male and female C57BL/6J mice (Jackson Laboratories, https://www.jax.org/strain/000664) in the present study. The mice were housed in a pathogen-free facility in humidity and temperature-controlled rooms maintained under a 12-h light/dark cycle. They were given free access to standard rodent chow and water. All experimental procedures were conducted according to NIH Guidelines for the Care and Use of Laboratory Animals. The Institutional Animal Care and Use Committee of the Medical University of South Carolina approved all the procedures.

2.2. Peptides, Nrf2 activators and Bach1 inhibitors

N,N'-(Naphthalene-1,4-diyl)bis(4-methoxybenzsulfonamide) (NMBSA) was purchased from Sigma-Aldrich (USA), 4-methyl-*N*-(quinolin-8-yl)benzenesulfonamide (8TQ), *N*-(quinolin-8-yl)-2,4,6-trimethylbenzenesulfonamide (8QBSA), *N*-(5-bromoquinolin-8-yl)-2,4,6-trimethylbenzenesulfonamide (Br-8QBSA), *N*-(5-chloroquinolin-8-yl)-2,4,6-trimethylbenzenesulfonamide (Cl-8QBSA) were purchased from ChemDiv (USA). CPUY192018, zinc protoporphyrin (ZnPP) were purchased from MedChemExpress (USA), tin protoporphyrin (SnPP) - from Cayman Chemical (USA). All other reagents were from Sigma-Aldrich (St Louis, MO). *N*-(2-(2-Hydroxyethoxy)ethyl)-1-methyl-2-((6-(trifluoromethyl)benzo[*d*]thiazol-2-yl)amino)-1*H*-benzo[*d*]imidazole-5-carboxamide (HPPE) (purity 99.8 %) was custom synthesized by Pharmaron (USA). See the structures of all compounds used in the study in Fig. S1A. Cell-permeable variants of Nrf2 peptides (purity >99 %) – YGRKKRRQRRRAQLQLD**EETGE**FLPIQ (wild-type), YGRKKRRQRRRAQLQLD**PETGE**FLPIQ (mutant), and YGRKKRRQRRRAQLQLD**PETGE**FLPIQK–NHCO–fumarate methyl (fumarate-linked peptide, >95 % purity) were custom synthesized by LifeTein LLC (NJ, USA). The peptides were tested in a fluorescence polarization (FP) assay using recombinant Keap1 to ensure no decrease in affinity for the Kelch domain occurred upon adding a TAT sequence to the ETGE motif peptides used in this work. The competitive displacement activity of cell-permeable peptides was evaluated using the Keap1-Nrf2 inhibitor screening assay kit (BPS Biosciences, San Diego, CA) according to the manufacturer's instructions, as previously described by us [9], which yielded dissociation constant (K_D) values within the 50–80 nM range.

2.3. Neh2-luc reporter assay

SH-SY5Y cell line stably expressing Neh2-luc [10] reporter was grown in DMEM/F12 supplemented with GlutaMAX (Thermo Fisher Scientific) containing 10 % FBS, 100 U/mL penicillin, and 100 μg/mL streptomycin) and plated into 96-well white flat-bottom plates at 15, 000 cells/well in 100 μL serum and incubated for 16 h at 37 °C, 5 % CO2. The small-molecule compounds were prepared as 10 mM stock solutions in dimethyl sulfoxide (DMSO). Then, the compounds were added to the wells, resulting in final concentrations ranging from 2.5 to 40 μM. Stock solutions of the peptides were prepared in 5 mM Tris-HCl buffer, pH 7.0, at concentrations of 4 or 8 mM, and were added to the wells to achieve the desired final concentration. The plates were incubated for 3 h at 37 °C. The media was removed, and cells were lysed with 20 μL of Lysis buffer (Promega) for 7 min at room temperature (RT). Luciferase activity was then measured using a GloMax multidetection plate reader (Promega) with 80 μL of BrightGlo™ reagent (Promega, Madison, WI). The reporter activation was normalized to the background (where only DMSO was added). Tert-butylhydroquinone (TBHQ) was used as a positive control. For the time-course experiments, 2 μL aliquots of the compounds or 5 μL aliquots of peptides were added to the wells at different time points, and the assay was conducted as described above. The experiments were performed in triplicate.

2.4. RT-PCR for Nrf2 target genes

Wild-type (WT) or Nrf2 knockout (KO) mouse embryonic fibroblast (MEF) was treated with wild-type TAT-Nrf2-peptide (200 μM) or *tert*-butyl hydroquinone (TBHQ, 20 μM) for 4 or 16h. Total RNA was isolated using TRIzol reagent (Invitrogen) according to the manufacturer's protocol. One μg of total RNA was reverse transcribed using a High-Capacity cDNA Reverse Transcription Kit (Invitrogen). cDNA was diluted, and 20 ng was used to amplify in an ABI prism 7900HT Real-time PCR system (Applied Biosystems) for transcripts of Nrf2 dependent genes: Heme Oxygenase 1 (HMOX1, 5′-GGGTGATAGAAGAGGCCAAGA-3′ and 5′-AGCTCCTGCAACTCCTCAAA-3′) and NAD(P)H quinone oxidoreductase 1 (NQO1, 5′-AGCGTTCGGTATTACGATCC-3′ and 5′-AGTACAATCAGGGCTCTTCTCG-3′) using Fast SYBR® Green Master Mix (Invitrogen). Cycling parameters were 95 °C for 10 s, followed by 60 °C for 1 min for 40 cycles. Relative expression was calculated using the ΔΔCt method [11]. Values are expressed as a fold of control reaction and normalized to beta-actin (Actb, 5′-CTAAGGCCAACCGTGAAAAG-3′ and 5′-ACCAGAGGCATACAGGGACA-3′) expression.

2.5. Keap1 and Nrf2 protein quantification assay

Since human and mouse Keap1 and Nrf2 have 94 % and 99 % homology, respectively, human recombinant Keap1 and Nrf2 proteins were used as standards and were produced as follows. The plasmids pET28a-His6-Halo-Tev-Keap1 and pET2-His6-Halo-TEV-Nrf2 were purchased from Addgene [12] and expressed in BL21(DE3) *E. coli cells* (C2527I, New England BioLabs), using 25 μM IPTG for induction. The bacterial pellet was collected and lysed in 50 mM Tris buffer, pH 8, containing 100 mM NaCl, 0.2 mg/ml lysozyme, and PMSF. His-tagged proteins were then isolated using the HisPur Ni-NTA purification kit (#88229, Thermo Scientific) with 200 mM Imidazole as the eluent in the same buffer. The eluted proteins were desalted using PD10 columns (#17-0851-01, GE Healthcare) and concentrated with Vivaspin6 30 kDa MWCO spin cartridges (28-9323-17, GE Healthcare). The protein concentrations of Keap1 and Nrf2 were determined using Nanodrop, taking into account the extinction coefficients of 13.8 and 8.58 at 280 nm, and the molecular weights of 106.6 and 104.72 kDa [13,13,13], respectively. Samples for western blotting were prepared from the Neh2-luc reporter line and untransformed SH-SY5Y cells grown in DMEM/F12 medium supplemented with 10 % fetal bovine serum (FBS) and antibiotics. For Neh2-luc, the media was supplemented with 500 μg/ml geneticin (G418, Sigma-Aldrich). Cell numbers were estimated with a TC10 cell counter (BioRad), and 100,000 cells were loaded per lane in a 12 % TGX gel. Tissue lysates were prepared in TNES (Tris 50 mM, NaCl 150 mM, EDTA 5 mM, SDS 1 %, NP-40 0.5 %, Na-deoxycholate 0.5 %, pH 7.4) buffer containing 1X protease inhibitor (P8340, Sigma), and the concentration was determined using the BCA assay. Brain regions (cortex and brainstem) and spinal cord were collected from young (3-month-old) or old (15-month-old) C57BL/6J mice. In 12 % TGX gels (Criterion, BioRad), 100 μg of brain lysates was separated along with standard proteins. Either 250, 100, 25, 10, 1, femtomoles of purified proteins were used as standards for Nrf2 and Keap1, respectively. After transferring to a nitrocellulose membrane, blots were probed for Keap1 (A21724, Abclonal) and Nrf2 (A0674, Abclonal) and detected using appropriate HRP-conjugated secondary antibodies. Band intensity was measured using ImageLab software (Bio-Rad).

2.6. RNA-seq and bioinformatics

Neuroblastoma SH-SY5Y cells were grown in 6-well plates in 2 mL medium per well up to 80 % confluence. Cells were treated with either 100 μM of the peptide or 5 μM HPPE, zinc, or tin protoporphyrin, and DMSO was used as a control. After 5 h of incubation, the media was removed, and the cells were washed three times with DPBS. They were then lysed in 700 μL QiaZol. RNA isolation was performed using the miRNeasy Micro Kit (Qiagen, Germany) according to the manufacturer's protocol. Nanodrop ND-1000 (Thermo Fisher Scientific, USA) was used to assess the quantity and purity of the extracted RNA. The quality control (QC) for the RNA was performed using an Agilent 2100 Bioanalyzer (Agilent Technologies, USA).

The libraries for mRNA sequencing were prepared from total RNA samples using the Illumina Stranded mRNA Library Prep Kit (Illumina, USA). Each sample was sequenced on the NextSeq 550 (Illumina, USA) to generate single-end 75-nucleotide reads. In the experiment with the small molecule compounds, the libraries for mRNA sequencing were prepared from total RNA samples using the MGIEasy RNA Library Prep Set (MGI Tech Co., China). The sequencing was conducted on the DNBSEQ-G400 (MGI Tech Co., China) to generate single-end 100-nucleotide reads.

The quality of FASTQ files was assessed with FastQC v0.11.9 (Babraham Bioinformatics, UK) and multiQC v1.9 [14]. The adapters were trimmed using FastP 0.21.1 [15]). The trimmed mRNA-seq reads were mapped to the reference human genome GENCODE release 37 (GENCODE GRCh38.primary assembly) using STAR 2.7.7a [16]. GENCODE release 37 genome annotation (gencode.v37.primary.assembly.annotation) [17] was used to generate the count matrix with the featureCount tool from subread-2.0.1 aligner [18,19].

The combined raw counts from RNA-sequencing data were processed for batch correction using ComBat [20]. Elbow-plot was used to determine the number of clusters for K-means clustering. Heatmaps were generated using the Interactive Complex Heatmap package [21]. We used Enrichr [22] to evaluate pathways affected in each cluster broadly. For WGCNA analysis, the RNA-sequencing data were normalized using the Variance Stabilizing Transformation (VST) of the DESeq2 package, and the 75th quantile normalized data were used to construct the networks [23,88]. The network was divided into modules based on correlation coefficient information at a soft power threshold of 10. We used dynamic tree cut to determine discrete modules containing genes with similar expression patterns, which were assigned an ID and color. After defining discrete modules using the dendrogram, we utilized the module Eigengene to correlate with the sample types and treatments (targets: Nrf2 or Bach1; treatments: Nrf2-peptide, HPPE, zinc-, and tin-protoporphyrin).

Differential expression analysis was conducted using DESeq2 v1.44.0. False discovery rates (FDRs) were calculated using the Benjamini–Hochberg procedure. To assess the statistical significance of differences in gene expression, FDR p-values with a threshold level of 0.05 were used. The statistical significance of gene set overlaps was assessed using the hypergeometric test, implemented with the "*phyper*" function in R (version 4.4.1). Gene Ontology enrichment analysis [24] (Gene Ontology et al., 2023) was performed with a built-in analysis tool on the GO web page [25]. The RNA-sequencing data generated in this study are available in the Gene Expression Omnibus (GEO) repository (GSE271364 and GSE287793).

2.7. Computer modeling

Small-molecule docking experiments were performed using the CDOCKER algorithm, as implemented in the Discovery Studio software suite (BIOVIA, San Diego, CA), followed by force field minimization and calculation of binding energies. The Nrf2 crystal structure with the bound inhibitor (4IQK.pdb) served as the starting template for this study. All ligands were imported and minimized using the 'Prepare ligands' protocol after adding hydrogen bonds. Force field minimization was performed using the molecular mechanics algorithm CHARMM, as implemented in Discovery Studio. A series of 50 positions was analyzed for each compound. The percentage of high-interaction energy positions that coincide with those of NMBSA in the crystal structure has been calculated and used as a comparative measure of compound affinity for the Kelch domain. Peptide docking experiments were performed using Discovery Studio, which employed the build protein and

superimposition tools (versus the initial peptide in the crystal structure 5WFV.pdb), followed by manual attachment of fumarate to the peptide chain. Final peptide pose selection was performed by applying CHARMM minimization algorithms. The Peptide docking benchmark was created using a set of Scoring and Analysis protocols. Docking energies for the versions of cell-permeable Nrf2 TAT-peptides studied in the work, in comparison to the control ETGE peptide, showed no principal change (Table S1).

2.8. Statistical analysis

Statistical analyses and graphs were performed using GraphPad Prism version 10.0.0 for Mac OS (GraphPad Software, San Diego, California, USA, www.graphpad.com). One-way or two-way ANOVA with appropriate post hoc analysis was used for multiple comparisons, whereas an unpaired, two-tailed Student's t-test was used for comparing two groups. All data were plotted as mean ± SEM and were considered significant when $P \leq 0.05$.

3. Results and discussion

3.1. Low effectiveness of true displacement activators in the cell-based assay

To demonstrate the differences in potency between alkylating/pro-oxidative and displacement activators, we used a fusion reporter constitutively expressing a protein fusion of the Neh2 domain of Nrf2 with firefly luciferase, Neh2-luc reporter (see Nrf2 and Keap1 domain structures in Fig. S2A and B, respectively). The Neh2-luc fusion protein is recognized by Kelch domains in dimeric Keap1 protein and undergoes ubiquitination and proteasomal degradation just like the endogenous Nrf2 (Fig. S2C). The advantage of the fusion reporter assay is its immediate response to the inhibitors of Nrf2-Keap1 interaction and the possibility of real-time monitoring of reporter activation [10]. Irreversible Nrf2 activators, such as bardoxolone and auranofin, the most potent alkylating agents that modify key Keap1 thiols, exhibit more than 20-fold activation of the reporter in the nanomolar range within 3 h of incubation (Fig. 1A). In contrast, less potent Nrf2 activators such as dimethyl fumarate (DMF) and *tert*-butylhydroquinone (TBHQ) work in the micromolar range (Fig. 1B). Irreversible modification by non-specific alkylating agents targets all active thiols present on cellular proteins, including Keap1, and results in the toxicity. However, the "benign" displacement activators, NMBSA and CPUY, exhibit EC_{50} values above 30 μM in the Neh2-luc assay (Fig. 1C), despite their K_D values being 1 μM and 40 nM, respectively, in the homogeneous cell-free fluorescence polarization assay (FP assay) [26]. The observed offset of EC_{50} by orders of magnitude for displacement activators (Fig. 1C) aligns with the published data on their biological activity in the ARE-luc assay and gene expression by RT-PCR [26] and is typical for all displacement activators see Ref. [27] references therein.

Another feature of displacement activators is the observed plateau (Fig. 1D), which never reaches the maximum activation threshold observed for irreversible activators (Fig. 1A and B), as one may expect for the truly reversible system that re-equilibrates [10]. The kinetic behavior of Neh2-luc reporter in the presence and absence of displacement activators can be quantitatively described due to its similarity to the actual endogenous mechanism of Nrf2 degradation (Fig. S3). Based on the steady-state concentration of all undegraded forms of luciferase fusion and the rate of luciferase fusion protein production determined as 60 nM and $M_o = 8$ nM/min, in Ref. [89], we calculated the rate-limiting step in Neh2-luc reporter degradation as $k_{lim} = k_1[\text{Keap1}] = 2.2 \times 10^{-3}$ s^{-1}. Using the published values for the rate constants of DLG and ETGE motifs binding to Kelch domain, determined by surface plasmon resonance [28], we took an estimate for the value of $k_1 = 4 \times 10^3\ M^{-1}s^{-1}$ and calculated the minimum concentration of Keap1 in cells as 0.55 μM (see legend to reaction 2 in Fig. S3). Thus, high intracellular concentrations of Keap1, a versatile adaptor that traps multiple protein clients into the Cul III ubiquitin ligase complex, could be the likely reason for the observed offset in the EC_{50} reported for displacement activators in the cell-based reporter assays. The amount of Keap1 protein clients

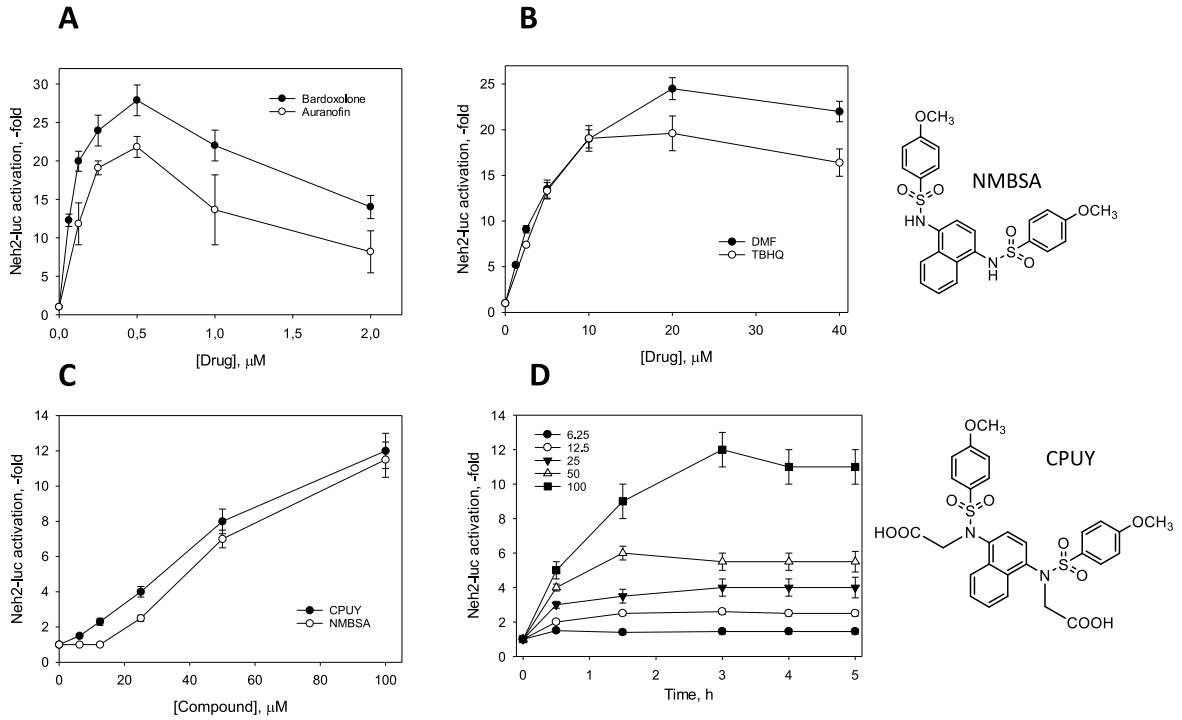

Fig. 1. Activation of Neh2-luc reporter with various Nrf2 activators. Luminescence is normalized to the background luminescence in the absence of an inducer. A: bardoxolone and auranofin; B: Dimethyl fumarate (DMF) and *tert*-butylhydroquinone (TBHQ); C: Displacement activators CPUY and NMBSA; End-point assay at 3 h incubation. D: Time-course of reporter activation with NMBSA. Mean±SEM.

competing in the cell with a displacement activator could have an additional effect on the biological potency of a displacement activator, depending on the absolute concentration of Keap1 client proteins and the activator's K_D value. The reported K_D values for ETGE and DLG Nrf2 peptides are 28 and 130 nM [28], respectively. Displacement activators should have a K_D in the same range or lower to successfully compete with homogeneous Nrf2 binding, and additionally, their concentration must match or exceed the intracellular concentration of Keap1. A third reason for the offset could be the non-specificity of displacement activators targeting the Kelch domain of Keap1, as there are at least 40 Kelch-domain-containing proteins in the human genome, as discussed in our recent review [29].

3.2. *High intracellular concentrations of Keap1 limit the effectiveness of displacement activators*

We determined the absolute amounts of intracellular Keap1 and Nrf2 in the untransformed neuroblastoma SH-SY5Y cell line and its transformed variant that stably expresses Neh2-luc fusion reporter using recombinant Keap1 and Nrf2 proteins. Our data demonstrate that expression of the Neh2-luc fusion protein in the Neh2-luc reporter cell line results in an increase in both Nrf2 and Keap1 protein levels (Fig. 2A). The endogenous Nrf2 is spared from degradation due to the constitutive synthesis of the fusion, which competes for Keap1 binding. Consequently, Nrf2 activation upregulates Keap1 through a positive feedback mechanism. In the Neh2-luc reporter cell line, compared to the untransformed cell line, the levels of Keap1 and Nrf2 proteins are ca. 5-fold and 2.5-fold higher, respectively (Fig. 2A and B). The Nrf2 content per 1000 cell is close to 0.1 fmol in the untransformed line and 0.25 fmol in the reporter line (Fig. 2A and B). Recalculated into absolute amounts, these numbers are equal to 60,000 molecules in the untransformed and 150,000 molecules in the reporter line. Our results are close to those previously reported for several cancer cell lines, where the absolute values for Nrf2 varied from 49,000 to 190,000 molecules per cell [30]. Considering the neuroblastoma cells in the monolayer are approximately 12 μm in diameter with a thickness of 3 μm, we estimated the volume of neuroblastoma cells as ca. 340 μm^3. Thus, the intracellular concentrations of Nrf2 are calculated as ca. 0.30 μM and 0.75 μM for the untransformed and the Neh2-luc reporter cell lines, respectively. The concentrations of Keap1 protein in the untransformed cell line of ca. 0.9 fmol per 1000 cell (540,000 molecules per cell) is increased up to 3.8 fmol (almost 2 million molecules per cell) in the reporter line, or from ca. 2.5 μM–12 μM (Fig. 2A and B). The number of Keap1 molecules in the untransformed neuroblastoma cell exceeds those reported for several cancer cell lines, where the absolute values for Keap1 varied from 45,000 to 300,000 molecules. However, the estimated Keap1 cytosolic concentration in RAW264.7 cells, calculated as 1 μM [30], is not far from the 2.5 μM determined in this study. Iso et al. reported no change in Keap1 amount when treated shortly with diethyl maleate, an electrophilic Nrf2 activator, a Michael acceptor that covalently modifies Keap1 cysteines, whereas Nrf2 protein levels rose from 330,000 to 710,000 molecules/cell [30]. However, we observed that the Keap1/Nrf2 ratio in the Neh2-luc reporter cells doubles compared to the untransformed neuroblastoma cell line (Fig. 2B) under basal conditions without any treatments, because of stable overexpression of the fusion protein. High Keap1 amount and rising Nrf2 protein levels explain why (1) irreversible alkylating activators elicit reporter activation in nanomolar concentrations and reversible displacement activators are active only at high

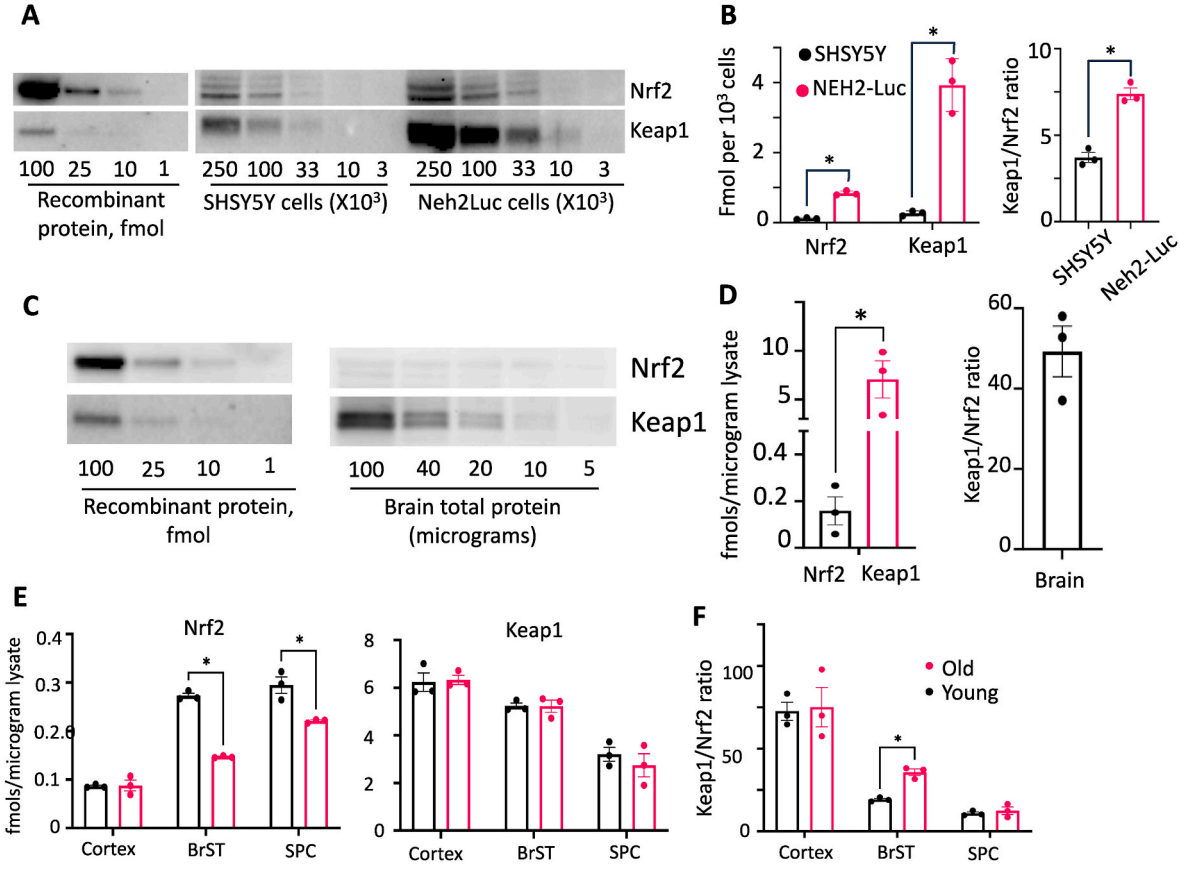

Fig. 2. Nrf2 and Keap1 protein content and their ratios in neuroblastoma (SH-SY5Y), Neh2-luc reporter lines, in the mouse whole brain, cortex, brainstem, and spinal cord.

Quantification of Nrf2 and Keap1 protein content and ratio in the untransformed neuroblastoma cell line (SH-SY5Y) and Neh2-luc reporter line (A, B), the mouse whole brain (A, C), and in the cortex, brainstem (BrST), and spinal cord (SPC) of young and old animals (D). Mean ± SEM.

micromolar concentrations: irreversible agents titrate Keap1 out stoichiometrically, whereas reversible activators displace the rising levels of endogenous Nrf2 from micromolar Keap1 levels (Fig. S3), and (2) Nrf2 displacement activators will never reach the maximum activation threshold of irreversible Nrf2 activators in the Neh2-luc assay: they cannot fully outcompete the rising Nrf2 levels from Keap1 and therefore simply shift the Nrf2-Keap1 binding equilibrium (see 12-fold activation in Fig. 1C, D versus 25-fold in Fig. 1A and B).

Given the high absolute amounts of Keap1 and Nrf2 in cancerous cell lines and high rates of Nrf2 production upon Keap1 inhibition, high-throughput screening for Nrf2 displacement activators in cell-based assays should be performed at high micromolar concentrations of drugs (20–100 μM). Genuine reversible displacement activators will exhibit high micromolar EC_{50} values in cell-based assays due to the aforementioned issues for fusion (Neh2-luc) and transcription reporters (ARE-luc). For example, a displacement activator – "Hit 1" (Fig. S1B) - identified and described in Ref. [31] showed K_D in homogeneous assay close to 1 μM and EC_{50} in ARE-luc assays of ca 12–18 μM, NMBSA exhibited cellular activity within 10–100 μM range [26] and CPUY within 1–100 μM [26]. An asymmetric NMBSA-type compound, RA839 (see Fig. S1B), showing K_D of 14 nM in FP assay, exhibited EC_{50} of ca. 40 μM in the cell-based ARE-luc assay [32]. A CPUY analog – compound K22 (see Fig. S1B) - with a tetramethylbenzene scaffold instead of a naphthalene [33] with $K_D = 180$ nM induced the expression of Nrf2 target genes at concentrations of 5–10 μM. In our earlier work on aspirin-containing prodrugs, an Nrf2 displacement activator with a naphthalene core, like NMBSA, and asymmetric aspirin-containing "arms" – Compound 9 (see Fig. S1B) was shown to behave as a potent displacement Nrf2 activator (EC_{50} of ca 10 μM in the reporter assay) due to partial hydrolysis catalyzed by the cell esterase, leading to a metabolite perfectly fitted into the Kelch domain - with C-docker energy twice as good as that for NMBSA [34]. In other words, if a prospective displacement activator shows EC_{50} below 1 μM in the cell-based reporter assay, an irreversible modification of Keap1 can be suspected.

To evaluate the prospects of genuine displacement activators for *in vivo* use, one must determine the absolute amounts of Keap1 and its major client protein, Nrf2, in tissues where oxidative stress is considered a key damaging factor and where the activation of the Nrf2 genetic program could be a "magic bullet." One of the most sought-after applications of Nrf2 activators is their potential to minimize oxidative stress in the brain, promoting healthy aging and counteracting age-associated cognitive decline. As shown in blots in Fig. 2C, D, the content of Nrf2 in brain is very low as compared to that of Keap1, almost 50 times lower (Fig. 2C). The reason for higher Keap1/Nrf2 ratio *in vivo* in the brain compared to cellular models may reflect the need in higher basal levels of Nrf2 to survive excessive ROS-production at non-physiological levels of oxygen in cell culture (ca. 21 %) than *in vivo* (ca. 2–9 %) [35]. The amount of Nrf2 varies from 0.1 to 0.2 fmol per μg protein or (Fig. 2C, D), which is ca 4–5 lower than the value reported for the rat brain in Ref. [36] as 0.8 μg/mg protein. To recalculate the values presented in Fig. 2C, D into the concentration units, one may consider the protein content estimate as 0.2 g/mL [37], and, thus, arrive at a concentration of ca. 0.02 μM Nrf2 and 1 μM Keap1 in the brain. The absolute amounts of Keap1 and Nrf2 proteins determined in young and old mice for three regions – cortex, brainstem, and spinal cord – are shown in Fig. 2E. No significant changes in Nrf2 and Keap1 content are observed in the cortex with aging. Interestingly, Nrf2 concentrations in brainstem and spinal cord are almost 3 times higher than in the cortex (close to 0.5 μM), whereas Keap1 content is lower, resulting in smaller Keap1/Nrf2 ratios in the brainstem and spinal cord than in the cortex (Fig. 2E). Importantly, aging results in a decrease in Nrf2 levels in the brainstem and spinal cord (Fig. 2E), and in the case of the brainstem, aging doubles the Keap1/Nrf2 ratio (Fig. 2F). Notably, early involvement of brainstem structures in the disease process has been described for PD and AD [38]. Neuropathological studies reveal that the tau pathology in prodromal and preclinical AD may originate in the brainstem nuclei [39]; the brainstem is a region that is compromised in early PD [40].

In all cases, a significant excess of Keap1 over Nrf2 in the brain opens an opportunity to upregulate the Nrf2 genetic program by targeting Keap1. However, for a displacement activator, micromolar concentrations may be required to be delivered into the brain to achieve optimal Nrf2 activation. In contrast, irreversible Nrf2 activators that are specific for Keap1 will be required in amounts matching those for Keap1-active thiols (ca. 20 nmol Keap1 in a 2 g brain). Under the most optimistic scenario, not accounting for the presence of multiple protein clients of Keap1 in the cell, one may expect an order of magnitude higher amounts of an Nrf2 displacement activator to be comparable to a hypothetical Keap1-specific irreversible inhibitor. In the recent work, CPUY molecule was modified by replacement of both carboxy-groups with amides and one of the *p*-methoxyphenyl substituents with a *p*-aminophenyl group to generate 2-((*N*-(4-((4-amino-*N*-(2-amino-2-oxoethyl)phenyl)sulfonamido)naphthalen-1-yl)-4-methoxyphenyl)sulfonamido)acetamide (coded as NXPZ-2, see Fig. S1B), a displacement activator with K_D of 94 nM and an improved ability to cross the BBB [41]. NXPZ-2 ameliorated learning and memory deficits following intracranial Aβ1-42- hippocampal injections in mice at doses ranging from 52 to 210 mg/kg [41]. These doses are higher than those typically used for dimethyl fumarate (DMF) in various scenarios of neurodegenerative diseases [42]. However, NXPZ-2 afforded benefits in the post-treatment scenario, with the drug administration starting 7 days after the Aβ1-42 injections [41]. In contrast, DMF and other alkylating Nrf2 activators are usually effective in a pretreatment regimen for therapeutic effects. Modifying the amine group in NXPZ-2 with a phosphodiester substitution (a novel variant named POZL, see Fig. S1B) further reduced the effective dose to less than 40 mg/kg [43]. However, the phosphodiester substitution is an active group, so the variant generated cannot be considered a "pure" displacement activator, especially given that the binding affinity for POZL for Keap1 is four times worse than that of NXPZ-2 [43]. Thus, POZL likely works through displacement followed by covalent modification.

The structural optimization of a displacement activator designed to lower the K_D to single-nanomolar values is insufficient because of the micromolar intracellular Keap1. Another concern is the possibility of non-specificity stemming from the existence of multiple Kelch-domain proteins. From this perspective, oxidative alkylating agents are more specific for Keap1, as it serves as a redox sensor and thus differs from other Kelch domain proteins. This dictates a different strategy for designing effective Nrf2 displacement activators intended for *in vivo* application – a combination of an Nrf2 displacement scaffold or peptide with an alkylating or pro-oxidative motif in a single molecule.

3.3. Targeting Keap1 with Nrf2 displacement activators bearing an alkylating motif

We developed a series of compounds combining a displacement scaffold with an alkylating motif attached. If one of the sulfonamide "arms" in NMBSA is removed and the naphthalene moiety is replaced with a quinoline, molecules like 8TQ and 8QBSA (Fig. 3) may also function as displacement activators. The quinoline scaffold preserves the affinity for the Kelch domain, and 8QBSA exhibits a reasonable value for C-docker energy (– 33 kJ/mol) by modeling studies. 8-Aminquinoline, by itself, exhibits some chemical activity compared to the inert naphthalene scaffold. The introduction of chloro- or bromo-substitution instead of the second "arm" in the 5th position creates a strong alkylating molecule preserving the ability to target Keap1 (Fig. 3B). Comparison of the 5-chloro-substituted analog 5-Cl-8QBSA with the 5-bromo-substituted analog 5-Br-8QBSA revealed that the presence of the larger halogen slightly reduces C-docker energy from −39 to −38 kJ/mol, respectively. Still, the energies are much closer to C-docker energy for NMBSA (−48 kJ/mol), used to validate the docking procedure (the docking model should overlap with the actual position of NMBSA in the crystal structure). Of note, the absence of the second

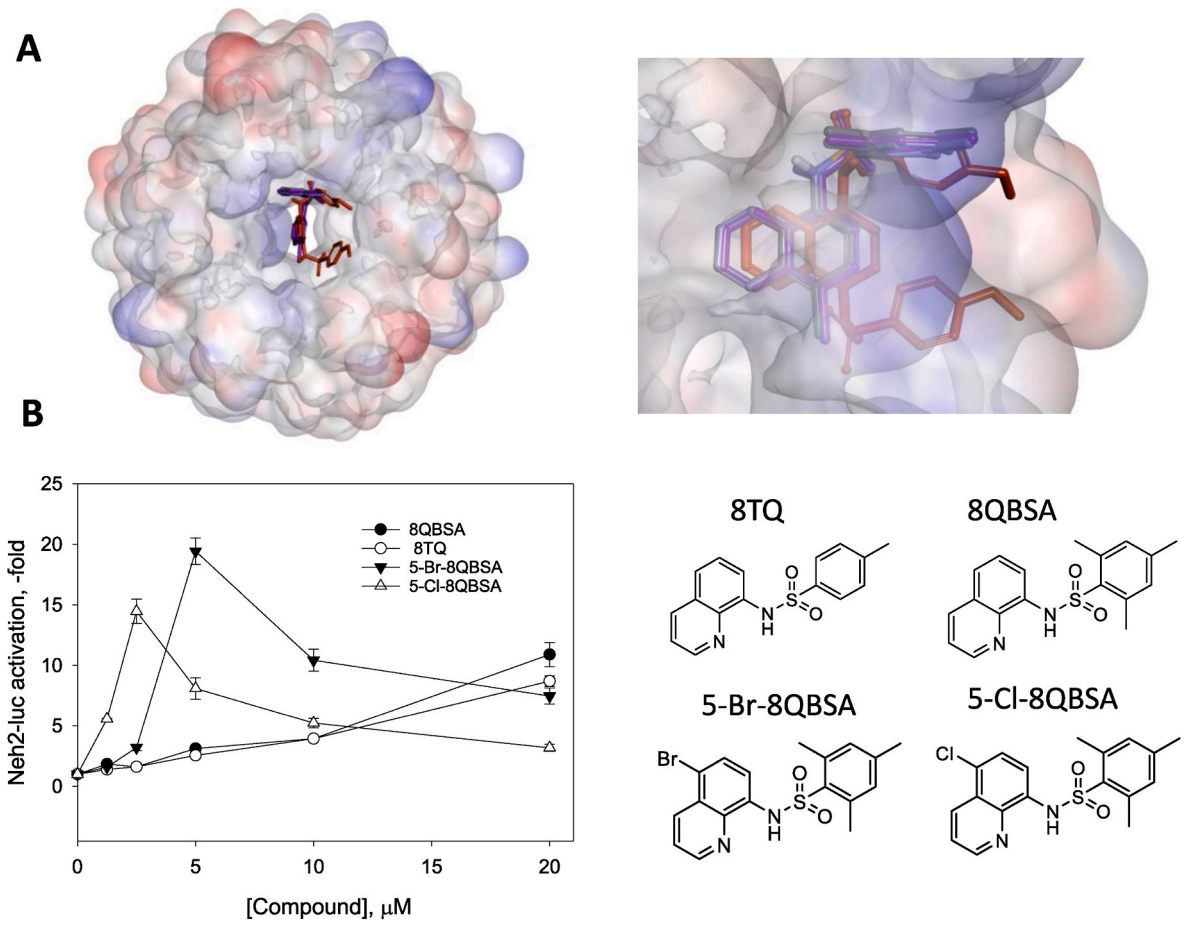

Fig. 3. Aminoquinoline activators of Nrf2. A: docking into the Keap1 Kelch domain. B: Neh2-luc reporter activation at 3 h incubation. The structures of pure displacement 8TQ and 8QBSA and alkylating displacement variants with halogen substitution in the 5th position – 5-Cl-8QBSA and 5-Br-8QBSA – are shown.

sulfonamide "arm" permits a deeper positioning of 5-halogenated analogs of 8-quinolinyl-benzenesulfonamide (8QBSA) (shown in purple) inside the Kelch pocket compared to NMBSA (shown in red in Fig. 3A). However, the introduction of a potent alkylating motif leads to unavoidable toxic side effects due to non-specific alkylation of cellular components on the way to the target. The activation profile exhibits a peak characteristic of the onset of toxicity (Fig. 3B). Several alkylating activators of Nrf2, including natural compounds (sulforaphane, myricetin, mangiferin, isoastilbin, and quercetin) as well as synthetic ones such as dimethyl fumarate and bardoxolone, protect against various diseases associated with inflammation. However, the exact mechanistic link between Nrf2 activation and its anti-inflammatory effects is not well understood [44]. 4-Methyl-*N*-(quinoline-8-yl)benzenesulfonamide, also known as 8-(tosylamino)quinoline (8-TQ), a mild Nrf2 activator similar to its 2,4,6-trimethyl-analog 8QBSA (Fig. 3B), has been demonstrated as an effective anti-inflammatory drug, which alleviated the signs of LPS-induced hepatitis in mice when administered at 20–40 mg/kg doses for 3 days [45]. However, the 8-aminoquinoline scaffold-derived drugs, despite their well-known use as antiparasitic drugs, are also known for serious side effects and are not a perfect choice for "benign scaffold" Nrf2 activators. Instead, by synthesizing asymmetric NMBSA-type compounds with a 4-amino-1-naphthol-based scaffold, the chemical reactivity can be increased due to the second "asymmetric" arm with a pro-oxidative motif, as exemplified by derivatives S47 [46] and 20c [47] (structures shown in Fig. S2B). Both molecules exhibit the properties of alkylating displacement activators providing targeted chemical modification of Keap1: S47 (Fig. S2B) with K_D of 1.9 μM is active at 4 μM in the cell [46]. The recently characterized compound ZJ01 (Fig. S2B) features a coumarin scaffold instead of a naphthalene and additionally bears substitutions with obvious alkylating potential (Fig. S2B). Although ZJ01 affinity for Keap1 drops (K_D is only 5.1 μM in FP assay), this compound exhibits an EC_{50} value of 8 μM *in vitro* in the cell-based assays, and is active *in vivo* at the 5–10 mg/kg doses in LPS-inflammation model on mice [48], thus providing strong evidence for the engagement of alkylating mechanisms.

3.4. Fumarate-linked Nrf2-peptide acts as a "pure" Nrf2 activator

To explore approaches that more closely mimic the endogenous scenario, we used a cell-permeable Nrf2 peptide construct featuring a 16-mer "ETGE" binding motif attached to the TAT-sequence, YGRKKRRQRRRAQLQLDE**ETGE**FLPIQ, named a wild-type Nrf2 peptide. The peptide is active in the Neh2-luc assay only above 50 μM: the reporter activation slowly develops and peaks at 6 h incubation and then declines, likely due to peptide degradation (Fig. 4A and B). The EC_{50} value in the reporter assay (ca. 200 μM) is orders of magnitude higher than the K_D estimate from the FP assay, and activation of Nrf2 target genes HMOX-1 and NQO-1 by the peptide at 200 μM is much less than that for a covalent activator, TBHQ, when used at 20 μM (Fig. 4C and D). The cell-permeable Nrf2 peptide triggers the Nrf2 genetic program only in cells expressing Nrf2, but not in Nrf2-deficient mouse embryonic fibroblasts (MEF) (Fig. 4C and D).

One could expect that mutations in the ETGE motif may improve the potency of the Nrf2 peptides in the cell-based assay based on the mutational analysis tested in the FP-assay: introducing proline ahead of the ETGE sequence instead of glutamic acid –DEETGEQ mutated to DPETGEL or DPETGEI, to match the sequence in p62, was reported to improve the K_D value by 50-fold [49]. However, such mutation

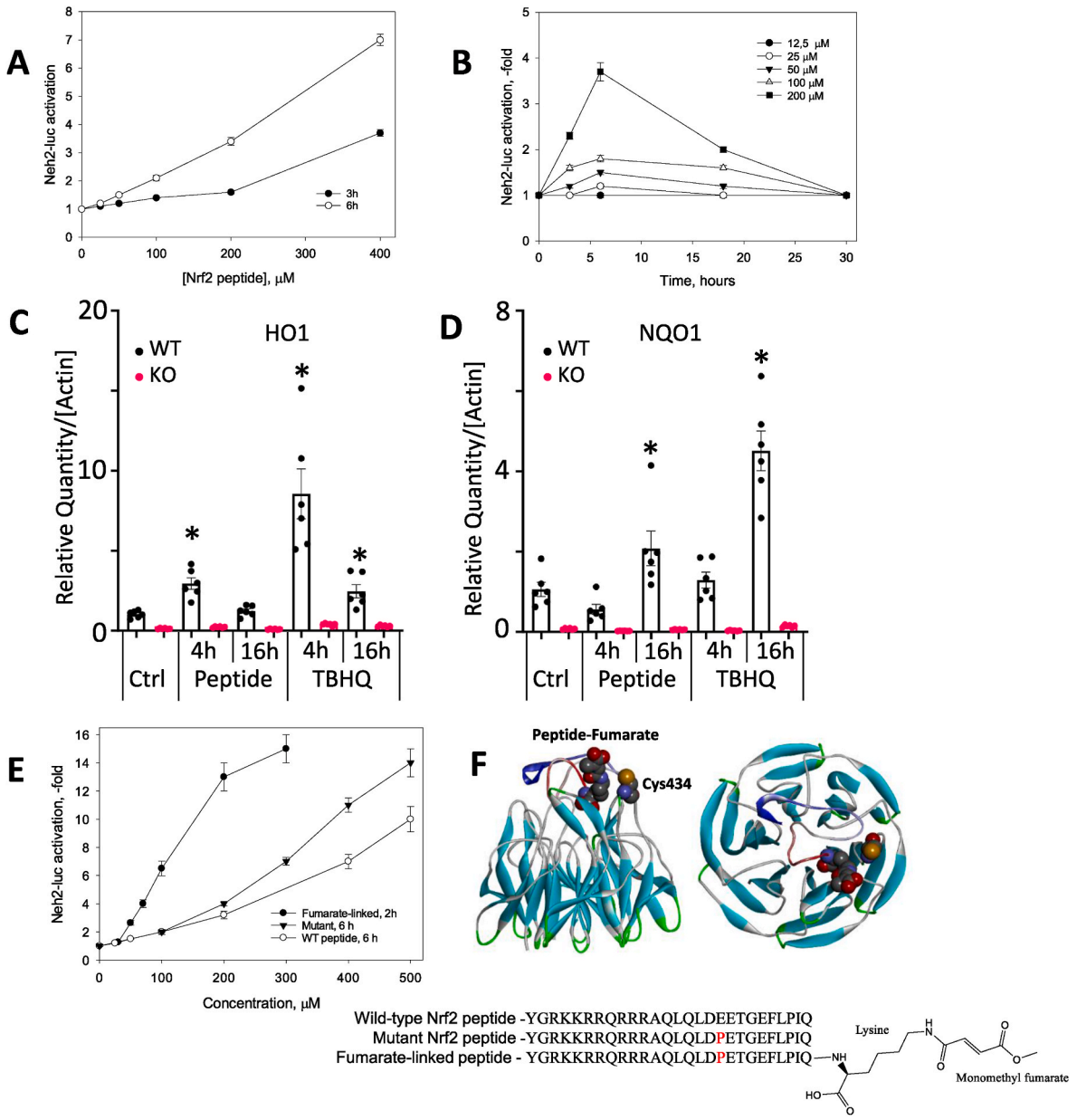

Fig. 4. Nrf2 activation with cell-permeable Nrf2 peptides. End-point (A) and time course (B) titration for the wild-type and Glu- > Pro mutant peptide; RT-PCR for Nrf2 target genes heme oxygenase 1 HO1 (C) and NQO1 (D) induced by 200 μM wild-type Nrf2 peptide at 4 and 16 h incubation in wild-type and Nrf2 KO mouse embryonic fibroblast in comparison to the action of 20 μM TBHQ; comparison of fumarate linked mutant Nrf2 peptide to the wild-type and mutant peptide without any alkylation motifs in Neh2-luc assay (E), and docking of fumarate-linked peptide into the Kelch domain showing Cys434 in close proximity to the fumarate tail (F).

introduced into the cell-permeable Nrf2 peptide – YGRKKRRQRR-RAQLQLD**PETGE**FLPIQ - showed a modest 2-3-fold improvement in EC_{50} in Neh2-luc assay (Fig. 4E). The values reported in the literature for the cell-permeable 14-mer TAT-Nrf2 peptide are $K_D = 22$ nM and $EC_{50} > 40$ μM for HMOX-1 induction [50] demonstrate a similar three orders of magnitude offset. This offset highlights both the issue with the high Keap1 content and the issue of reversible competition with the endogenous Nrf2, which is likely to exhibit a significantly higher affinity for Keap1 in the cell than the one measured in the FP assay. We must note that there are two Kelch sites in the Keap1 dimer, and endogenous Nrf2 binds to both Kelch sites cooperatively. Stated another way, the local concentration of Nrf2 after dissociation from one of the two Kelch sites in the Keap1 dimer is high compared to the free concentration of a "displacement" activator. Because of this, the mean complex lifetime for Nrf2 will be much longer than the mean complex lifetime of univalent "displacement" activators. A recently reported multivalent "displacement" activator employs a synthetic, lipophilic polymer backbone with the LDPETGEFLRRRR peptide on each monomer unit [51]. An increase in local concentration of the Nrf2 peptide comes at the expense of its high molecular weight (10–15 kDa, depending on the degree of polymerization). Again, these polymers, which contain repeating Nrf2 peptide fragments, exhibit a sub-nanomolar affinity for the Kelch domain in an FP assay but yield micromolar values in the ARE-luc assay in HepG2 cells. The values of EC_{50}, being recalculated for the concentration of the peptide, give EC_{50} of 60–100 μM per peptide link for low (11 monomers) and high (27 monomers) polymerization degree variants, respectively (see Fig. S28B in Ref. [51], just slightly better values than those observed in Fig. 4A and B.

Two other issues limit the use of peptides, namely, a low permeability through the membrane and instability within the cell. In the above paper [51], with the help of a properly modified peptide sequence (quadrupole arginine residues at the C-terminus of the Nrf2 peptide) and

polymer backbone, these issues were resolved, and the subsequent use of the polymeric Nrf2 peptide as a single intravenous injection demonstrated a promising therapeutic effect in the post-treatment regimen in a myocardial infarction rat model [52]. Despite the problems associated with the use of peptides, *in vivo* studies with Nrf2-peptides show that such treatment is truly benign and effective in post-treatment regiments: DEETGE-CAL-Tat peptide (NH2-RKKRRQRRR-PLFAER-LDEETGEFLP--CONH2) [53] in a rat model of global cerebral ischemia demonstrated a robust neuroprotection and preservation of hippocampal-dependent cognitive function, both at doses 30–100 μg in 5 μl of 0.9 % saline injected by unilateral intracerebroventricular administration 30 min before ischemia and at doses 1–2 mg in 100 μl of saline (120 and 240 μg/d) 1–9 days post-treatment, beginning at 1 d after reperfusion.

Given the reversible mechanism of Nrf2 peptide action, linking the peptide to a chemical moiety with an alkylating or pro-oxidative motif may create an irreversible Keap1-targeted Nrf2 activator. To minimize side effects, the alkylation agent has yet to be activated or released from the peptide in the cell. A good candidate for such a mechanism could be monomethyl fumarate: a methyl fumarate-bound cell-permeable Nrf2 peptide synthesized by the addition of a lysine residue to the C-terminal of the mutant Nrf2 peptide via an amide bond (see structure in Fig. 4F). The nature of substitutions at the fumarate carboxy group strongly affects its cell-permeability and alkylating potency, with monomethyl fumarate (MMF) exhibiting the lowest potency in the cell-based assays (MMF ≪ DMF < diethyl fumarate < bis-salicyl fumarate) [54]. Peptide-bound methyl fumarate will be slowly hydrolyzed to become an active alkylating agent in the cell. In this way, it may have sufficient time to target Keap1 before turning into a potent alkylating agent. Hence, the off-target effects of fumarate will be minimized. As shown in Fig. 4E, the fumarate-linked Nrf2 peptide exhibits a lower EC_{50}; more importantly, it reaches the plateau of maximum activation within 2 h. Computer modeling points to Cys 434 residue neighboring to C-terminal fumarate in the designed Nrf2 peptide (Fig. 4F). Therefore, there is a potential alkylation target in the Kelch domain right at the Nrf2 peptide binding site.

If a fumarate-linked Nrf2 peptide functions as a Keap1-specific alkylating agent, one would expect it to activate the Nrf2 genetic program selectively, i.e., it would behave as a perfect Nrf2 activator. We performed transcriptomic analysis to investigate the specificity of the Nrf2-peptide in SH-SY5Y cells. We found that GO analysis identifies only one biological process activated by the Nrf2-fumarate peptide (Fig. 5) – "cellular response to oxidative stress." The list of top-activated genes is presented in Table 1, and the genes can be divided into four subgroups: (1) antioxidant defense, (2) aggregate clearance, (3) membrane interactions and signal transduction, and (4) glycolysis. The first subgroup of activated proteins/enzymes in antioxidant defense is represented by eight genes, with **OSGIN1** (oxidative stress-induced growth inhibitor 1) activation being most pronounced. **SRXN1 (**Sulfiredoxin-1), **SLC7A11** (cystine-glutamate antiporter), **TXNRD1** (thioredoxin reductase 1), **GSR (**glutathione reductase), **NQO-1** (inducible cytosolic NAD(P)H-quinone

Table 1
Major upregulated genes for cell-permeable fumarate linked Nrf2 peptide.

Gene	Gene Product	Nrf2-Fumarate Peptide	HPPE
Antioxidant Defense			
OSGIN1	Oxidative stress induced growth inhibitor 1	13.90	12.30
SRXN1	Sulfiredoxin-1	7.47	3.19
SLC7A11	Cystine-glutamate antiporter	6.37	11.30
TXNRD1	Thioredoxin Reductase	4.54	3.34
NQO1	NAD(P)H-quinone oxidoreductase 1	4.25	5.61
GCLM	Gamma-glutamyl cysteine synthetase	3.87	5.90
HMOX1	Heme oxygenase 1	2.18	64.7
GSR	Glutathione Reductase	2.14	1.69
LUCAT1	Lung cancer-associated transcript 1	3.32	14.7
Protein aggregate clearance			
SQSTM1	Ubiquitin-binding protein p62	2.51	2.41
DNAJB4	Heat shock protein 40 (homolog)	2.28	2.76
PSMA6	Proteasome Alpha-subunit type 6	2.25	<1.5
RPS23	Small ribosome protein 23	1.90	<1.5
GABARAPL1	GABA type A receptor associated protein like 1	1.74	1.93
Signal transduction and membrane transport			
P2Y6	Pyrimidinergic receptor P2Y6	2.64	3.33
PANX2	Pannexin 2	2.44	2.50
PALM3	Paralemmin-3	2.30	1.75
ABCC3	ATP binding cassette subfamily C member 3	1.73	4.93
ABCB6	ATP binding cassette subfamily B member 6	1.74	1.98
Glycolysis			
ALDOA	Aldolase A	2.98	<1.5
ME1	Malic Enzyme 1	2.05	2.33
Feedback regulation			
BACH1	Transcriptional repressor of Nrf2	1.58	2.01
BACH2	Transcriptional repressor of Nrf2	1.59	2.04

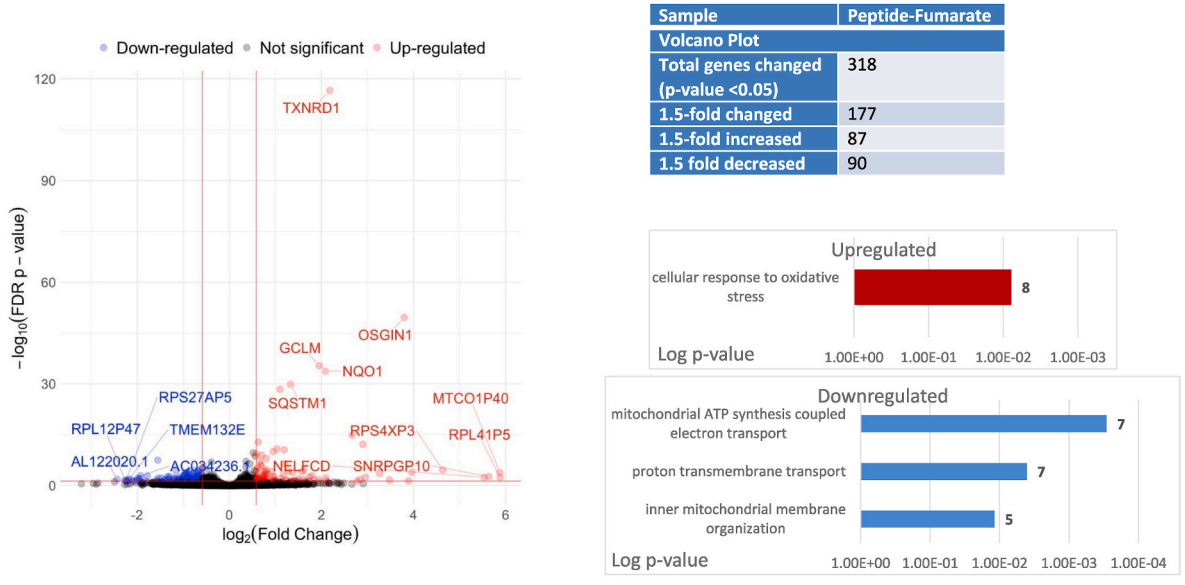

Fig. 5. Volcano plot and affected GO Biological Processes in neuroblastoma cells treated with 100 μM cell-permeable fumarate-linked Nrf2 peptide at 5 h incubation.

oxidoreductase 1), **GCLM** (the regulatory subunit of gamma-glutamylcysteine synthetase), **HMOX1 (**the inducible heme oxygenase 1) are well-known Nrf2 targets. **LUCAT1** - long noncoding RNA - was only recently shown to play a protective role in oxidative stress injury, inflammation, viability, and apoptosis of cardiomyocytes induced by H_2O_2 via regulating miR-181a-5p [55].

The second subgroup includes **SQSTM1 (p62),** another Keap1 client protein, known as a cellular "garbage collector" that binds to ubiquitinated protein aggregates and delivers them to the autophagy machinery for disposal. Disruption in the p62-autophagy system is a hallmark of neurodegenerative diseases such as Alzheimer's, Parkinson's, Huntington's, and amyotrophic lateral sclerosis [56]. The other targets are much less explored such as: **DNAJB4** encoding a heat shock protein 40 homolog, likely functions as a chaperone, exhibits anti-apoptotic properties [57], and interacts with E-cadherin [58], the mu-opioid receptor OPRM1, and protein SDIM1 [59]; the downregulation of the latter is associated with AD. **PSMA6** encodes alpha-6 subunit of the 20S proteasome, whose inhibition leads to proteasome dysfunction, as observed in diabetic nephropathy [60], and is a potential target of the Nrf2 transcription factor. **RPS23** codes for small ribosomal protein 23, a hub protein associated with the formation of neurofibrillary tangles in AD [61]. It is a substrate for prolyl hydroxylase OGFOD1 [62], and when hydroxylated, it loses its protective function; the OGFOD1 enzyme inhibition with Roxadustat (FG-4592) is, in fact, the main reason for the drug's protective effect in ischemia-reperfusion [63]. GABARAPL1 is an autophagy-associated protein and, like GABARAP, promotes $GABA_A$ receptor clustering [64]. Low expression of GABARAPL1 decreases sensitivity to ferroptosis in cancer stem cells [65]. The **P2Y6** gene encodes the $P2Y_6$ receptor, which appears to mediate Aβ- and tau-induced neuronal and memory loss through the microglial phagocytosis of neurons [66]. P2Y6R may have a detrimental or beneficial role in the nervous system in the context of neurological pathologies, such as ischemic stroke, AD, PD, radiation-induced brain injury, and neuropathic pain [67].

The third subgroup of targets includes signal transduction and membrane interaction players. **PANX2 (Pannexin 2)**, located at the interface between mitochondria and the endoplasmic reticulum [68], is particularly abundant in the brain. A link between Nrf2 activation and PANX2 induction under the action of oltipraz was reported in Ref. [69], and PANX2 was confirmed as an Nrf2 target gene and one of the risk genes for autism spectrum disorder [70]. **PALM3** codes for parallemmin-3, a phosphoprotein with prenyl and palmitoyl substituents, providing its interaction with the cytoplasmic side of the cell membrane and thus participating in neuronal membrane dynamics [71]. **PALM3** was never reported as an Nrf2 target gene. **ABCB6** and ***ABCC3*** *transporters* are linked to heme/iron homeostasis: **ABCB6** transports a broad spectrum of porphyrins, and ABCB6 knockout mice exhibit an increased auditory brainstem response threshold, resulting in reduced hearing sensitivity, thus pointing to the ABCB6 role in inner ear development and function [72]. ***ABCC3*** acts as an overflow pump for bile acids and glucuronide conjugates of bilirubin and drugs [73]. One of the limitations of this study is that the transcriptomic analysis was performed in cell lines grown at non-physiological levels of oxygen (ca. 21 %). However, on the other hand, Nrf2 is known to interact with Hypoxia-inducible Factor-1α (HIF-1α), which becomes activated at physiological oxygen (2–9 %), therefore non-physiological oxygen levels in cell-lines allow identification of select Nrf2-target genes in transcriptomic analysis [74]. Thus, the list of genes activated by the cell-permeable Nrf2 peptide belongs solely to the Nrf2-genetic program. Many of these genes are well-characterized; however, this list also includes several novel yet uncharacterized Nrf2 target genes.

3.5. Comparative transcriptomic analysis reveals that HPPE is both an Nrf2 activator and a Bach1 inhibitor

Feedback regulation of Nrf2 is achieved through Keap1, which regulates Nrf2 protein stability, and through Bach1 and Bach2 transcriptional repressors of Nrf2 [3]. Bach1 and Bach2 genes are modestly upregulated at 5 h following incubation with fumarate-linked Nrf2 peptide (Table 1). Feedback regulation prevents the possibility of reductive stress, which is typical for the use of stoichiometric reducing agents like dithiotreitol, ascorbic acid, vitamin E, or, in the case of mutations, preventing Nrf2 from degradation by Keap1 [75] and Cullin III ubiquitin ligase [76]. One of the main features of neurodegenerative diseases is the dysregulation of redox homeostasis, which leads to the accumulation of oxidative damage. While increased oxidative stress is known to upregulate Nrf2, this increase in Nrf2 is insufficient to combat ongoing neurodegeneration due to upregulation of its transcriptional repressor Bach1, which would inhibit the Nrf2 signaling [77]. Therefore, for sustained activation of Nrf2, which is essential for treating chronic diseases, Bach1 inhibition in conjunction with Nrf2 activation is critical. Heme (iron protoporphyrin) is a natural regulator of Bach1, inhibiting its transcriptional activity and providing its export from the nucleus, followed by proteasomal degradation [78]. Other transition metal protoporphyrins, such as zinc- and tin-protoporphyrins, are known to inhibit Bach1 transcriptional repression by targeting Bach1 for degradation, similar to heme [9,79,80], and are commonly used as Bach1 inhibitors or derepressors. HMOX1 is a classical target gene of the Nrf2/Bach1 couple. HPPE is one of the recently identified HMOX1 activators that exhibit both Nrf2 activation and Bach1 inhibition properties [9,81]. While HPPE is not an alkylating agent, it is still active in the Neh2-luc assay and thus directly stabilizes the Nrf2 protein [9]. The mechanism by which HPPE stabilizes Nrf2 is currently the focus of research in our laboratory. The recently proposed mechanism of Nrf2 activation based on the HPPE property to act as a zinc ionophore [82] is doubtful, as we failed to observe an effect of zinc in the Neh2-luc reporter for HPPE-induced activation (Fig. S4). Further, incubation with 1 mM N-acetylcysteine failed to quench Neh2-luc activation by HPPE (Fig. S4), which suggested that HPPE-induced Neh-2 luc activation was not the result of alkylation of Keap1 thiols. To evaluate whether the transcriptomic landscape of HPPE-treated cells aligns more closely with that of classical Nrf2 activators, such as cell-permeable Nrf2 peptide, or with Bach1 inhibitors like zinc and tin protoporphyrins, we employed RNA-sequencing analysis.

A comparative transcriptomic analysis of HPPE action in SH-SY5Y neuroblastoma cells demonstrates that HPPE possesses both activities. The Venn diagrams for HPPE and the two porphyrins (Fig. 6A and B) show quite an intersection with Bach1 inhibitors (71 common activated genes in Fig. 6A, see the list in Table 2) and some intersection with Nrf2-peptide (22 upregulated common genes in Fig. 6C). The list of these genes matches "Nrf2 only" target genes identified with cell-permeable fumarate linked Nrf2 peptide (Table 1). The statistical significance of these gene set intersections was confirmed by hypergeometric testing (Table S3). The K-means clustering analysis was performed using the empirical number of the clusters based on elbow plot (Fig. S5A). The clustering analysis demonstrated that, except for a small population of genes in cluster number 3 (Fig. 7A dotted box: Fig. 7B and Fig. S7), HPPE treated SH-SY5Y cells clustered with zinc and tin protoporphyrins. This gene signature in cluster 3 was enriched for canonical Nrf2/Bach1 pathways (Fig. S5B). However, the transcriptional landscape of HPPE-treated cells predominantly matched with the transcriptional landscape of zinc and tin-protoporphyrins than those compared to the Nrf2-peptide-treated cells in the top 2000 variable genes (Fig. 7A). Interestingly, cluster 4 with Bach1 inhibition effects (HPPE and protoporphyrin's) was enriched for neuroactive ligand-receptor interactions (Fig. S5B) indicating a non-canonical role of Bach1 in neuronal physiology independent of Nrf2. These results were further confirmed by employing weighted gene co-expression network analysis (WGCNA) in all observed modules (Fig. S6A–D). Differential gene expression analysis using DEseq2 between HPPE, Nrf2 peptide, zinc and tin-protoporphyrin (FDR $q < 0.1$, Log2FC = 2) demonstrated 1577 differentially regulated genes between HPPE and Nrf2-peptide treated

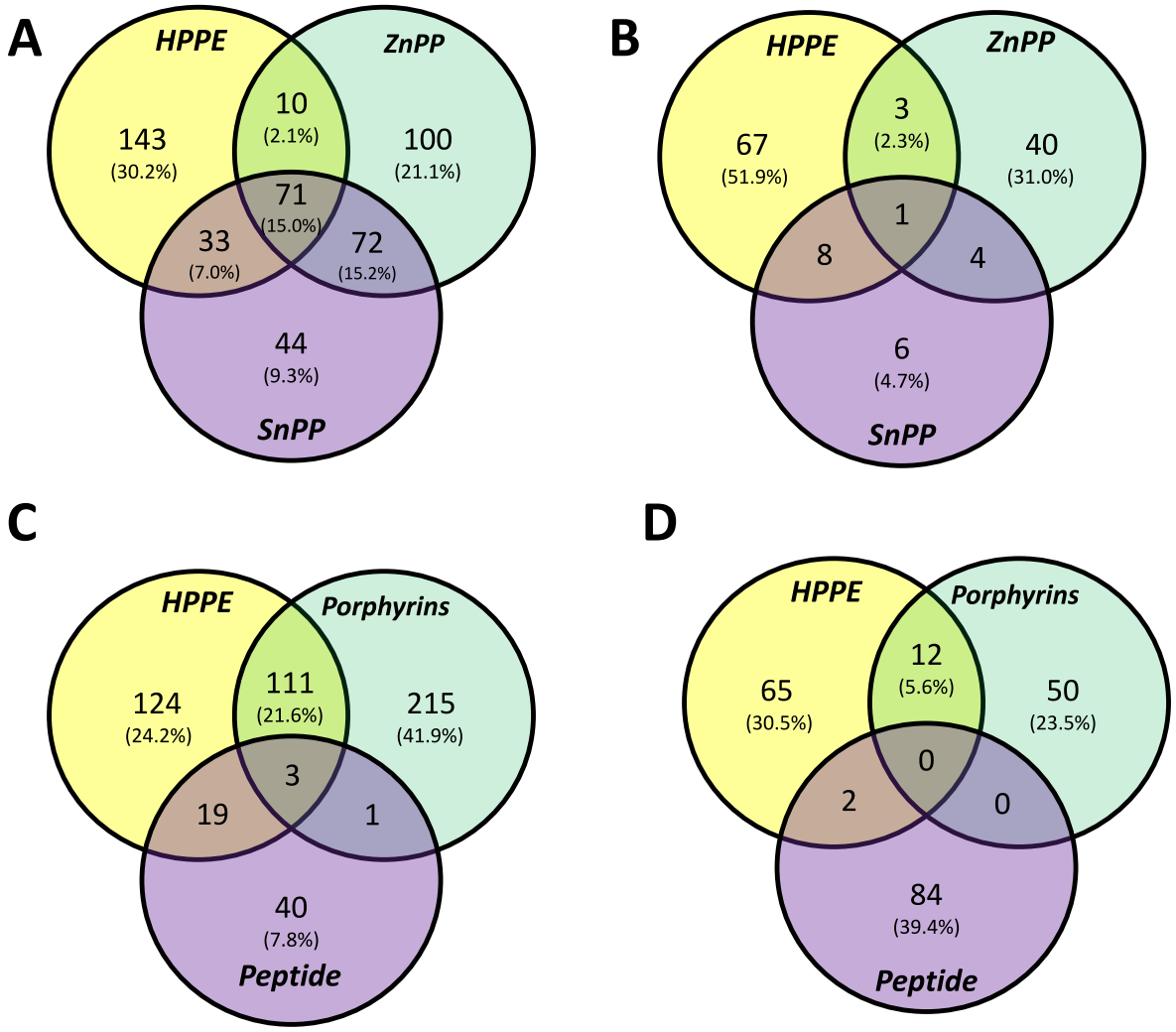

Fig. 6. Venn diagrams for upregulated (A, C) and downregulated (B, D) genes for neuroblastoma cell line treated for 5 h with the following compounds: HPPE, Zinc (ZnPP), and tin (SnPP) protoporphyrins at 5 μM each and 100 μM of cell-permeable fumarate-linked Nrf2 peptide.

cells, whereas 9 differentially expressed genes between HPPE and (zinc & tin-protoporphyrin) (Fig. 7C), further confirming the similarity of HPPE with Bach1 inhibitors. Overall, the transcriptomic analysis demonstrates that HPPE is a Bach1 inhibitor, very similar to the known metal protoporphyrin inhibitors of Bach1, and it also activates the Nrf2 genetic program, like the cell-permeable Nrf2 peptide.

4. Conclusions

Nrf2 signaling plays a crucial role in maintaining the redox balance. Previous studies have reported contradictory effects of aging on the expression of Nrf2 in animals [83]. For instance, some studies have shown that brain and spinal cord samples from aging mice showed a decline in Nrf2 activity [84,85] while others report the opposite [86]. Here we analyze, for the first time, the absolute content of Nrf2 and Keap1 proteins in human neuroblastoma cell lines and in discrete regions of the mouse brain, as a function of age. We demonstrate brain-region-specific decline in the Nrf2 signaling during aging. The Nrf2 level in the brainstem, a region critically vulnerable to PD, was significantly lower in the aged mouse, tipping the Keap1/Nrf2 ratio further in favor of Keap1. The spinal cord similarly exhibited a decrease in Nrf2 expression during aging, while levels of both Nrf2 and Keap1 remained unaltered in the cortex. Our results also suggest that the relative expression of Nrf2 and Keap1, rather than either protein in isolation, is crucial for understanding physiological relevance. Therefore, despite the aging-related dip in Nrf2 expression in the spinal cord, the relevance of Nrf2 downregulation in the midbrain is more significant. The uneven loss of the Nrf2 activity can elicit region-specific susceptibility to oxidative stress in the brain. Intriguingly, the midbrain, which is most susceptible to the loss of Nrf2 expression, is also the most vulnerable region to neuronal loss in PD, a disease strongly associated with oxidative stress [87].

The development of Nrf2 activators suitable for treating chronic age-related conditions and diseases, therefore, necessitates addressing several issues stemming from the mechanistic aspects of Nrf2 stabilization and activation. First, a high intracellular concentration of Keap1 protein sets the limit for the efficiency of reversible displacement activators, as their EC_{50} will always exceed the 1 μM level, independent of their K_D value. Second, Keap1 is an adaptor protein for a dozen client proteins for the Cullin III ubiquitin ligase complex. As such, the displacement activator must outcompete endogenous Nrf2 and all other client proteins, which provides an additional offset in EC_{50} values, shifting them to ca. 5–10 μM or above. Third, as we discussed earlier, there may be a significant abundance of other off-target Kelch-domain proteins that could interact with a displacement activator designed to interact with the Kelch domain [29]. All these factors contribute to the observed offset of biologically effective concentrations of displacement activators by many orders of magnitude compared to their binding constants determined in an FP assay. The redox-sensing nature of Keap1 is a distinct characteristic that can be used to discriminate Keap1 from

Table 2
Overlapping upregulated genes for HPPE, zinc, and tin protoporphyrins.

Gene symbol	Gene product	HPPE	ZnPP	SnPP
MALL	mal, T cell differentiation protein like	80.65	44.31	65.06
LIF	LIF interleukin 6 family cytokine	5.28	3.31	6.91
SPOCD1	SPOC domain containing 1	5.12	4.60	5.29
SIRPG-AS1	SIRPG antisense RNA 1	4.95	9.97	9.21
CEBPD	CCAAT enhancer binding protein delta	4.52	3.31	3.61
FOSL1	FOS like 1, AP-1 transcription factor subunit	4.45	1.97	2.98
INSYN2B	inhibitory synaptic factor family member 2B	4.32	4.05	4.57
CMKLR1	chemerin chemokine-like receptor 1	4.05	3.15	4.52
PTGS1	prostaglandin-endoperoxide synthase 1	4.03	2.48	3.45
SERPINE1	serpin family E member 1	3.91	2.14	2.28
FLT1	fms related receptor tyrosine kinase 1	3.85	3.22	3.76
ANKRD1	ankyrin repeat domain 1	3.50	2.50	2.89
SPRY1	sprouty RTK signaling antagonist 1	3.34	2.78	3.38
CCN1	cellular communication network factor 1	3.21	1.68	2.40
HSPB8	heat shock protein family B (small) member 8	3.20	1.85	2.14
PLAT	plasminogen activator, tissue type	3.19	1.87	2.23
SLC12A8	solute carrier family 12 member 8	3.11	2.23	2.25
UBASH3B	ubiquitin associated and SH3 domain containing B	3.02	2.93	2.96
SYNJ2	synaptojanin 2	2.97	2.71	2.44
FAM83G	family with sequence similarity 83 member G	2.81	1.63	1.78
EDN1	endothelin 1	2.76	3.65	5.68
FAM30A	family with sequence similarity 30 member A	2.70	2.60	3.20
CYTOR	cytoskeleton regulator RNA	2.58	2.70	2.27
TFPI2	tissue factor pathway inhibitor 2	2.57	2.16	2.59
SPHK1	sphingosine kinase 1	2.53	1.99	2.53
RGS3	regulator of G protein signaling 3	2.39	1.65	1.81
DKK1	dickkopf WNT signaling pathway inhibitor 1	2.36	1.62	2.15
GREM1	gremlin 1, DAN family BMP antagonist	2.34	2.26	2.42
ELL2	elongation factor for RNA polymerase II 2	2.33	2.14	2.24
SYT12	synaptotagmin 12	2.28	2.94	3.48
SGK1	serum/glucocorticoid regulated kinase 1	2.28	1.55	1.67
ZYX	zyxin	2.26	1.90	2.61
ITGA2	integrin subunit alpha 2	2.25	2.14	2.49
DKK2	dickkopf WNT signaling pathway inhibitor 2	2.25	2.33	2.62
PTX3	pentraxin 3	2.23	2.05	3.51
CD274	CD274 molecule	2.16	2.16	2.84
CXCL12	C-X-C motif chemokine ligand 12	2.13	1.58	1.95
FGF5	fibroblast growth factor 5	2.13	2.69	2.72
EVA1A	eva-1 homolog A, regulator of programmed cell death	2.12	1.94	2.40
TGFB1I1	transforming growth factor beta 1 induced transcript 1	2.12	1.60	1.92
PLK2	polo like kinase 2	2.12	1.56	1.66
TGM2	transglutaminase 2	2.12	2.00	2.20
ITGA6	integrin subunit alpha 6	2.11	1.88	2.42
SH3TC1	SH3 domain and tetratricopeptide repeats 1	2.10	1.72	1.78
IL4R	interleukin 4 receptor	2.09	2.37	2.85
THBS1	thrombospondin 1	2.05	1.60	1.98
FHL2	four and a half LIM domains 2	2.04	1.67	1.95
NEAT1	nuclear paraspeckle assembly transcript 1	2.03	1.96	2.01
MIR4435-2HG	MIR4435-2 host gene	1.99	2.11	1.68
TRAF1	TNF receptor associated factor 1	1.94	3.55	3.75
FLNC	filamin C	1.93	1.82	1.82
KLF6	Kruppel like factor 6	1.86	1.73	1.91
CREB5	cAMP responsive element binding protein 5	1.84	2.01	1.72
MIR23AHG	miR-23a/27a/24-2 cluster host gene	1.77	1.56	1.81
RYR3	ryanodine receptor 3	1.75	2.18	1.68
AOPEP	aminopeptidase O (putative)	1.75	1.95	2.04
TMC6	transmembrane channel like 6	1.74	1.58	1.64
FBLIM1	filamin binding LIM protein 1	1.73	1.84	1.97
LDLR	low density lipoprotein receptor	1.70	1.90	1.90
TNS1	tensin 1	1.69	1.89	1.85
ERRFI1	ERBB receptor feedback inhibitor 1	1.66	1.58	2.12
PHLDA1	pleckstrin homology like domain family A member 1	1.64	1.72	1.91
FOSL2	FOS like 2, AP-1 transcription factor subunit	1.63	1.58	1.51
XYLT1	xylosyltransferase 1	1.62	1.79	2.10
HSPB7	heat shock protein family B (small) member 7	1.62	1.50	1.53
AC244033.2	NA	1.60	1.61	1.66
RFTN1	raftlin, lipid raft linker 1	1.59	1.57	1.53
VCL	vinculin	1.58	1.62	1.63
IQGAP2	IQ motif containing GTPase activating protein 2	1.58	1.88	1.59
AL392083.1	NA	1.50	1.59	1.61

other Kelch domain-containing proteins in the cell. Therefore, a combination of a displacement scaffold with a pro-oxidant or alkylating motif may solve the problem of Keap1-specific targeting and efficient inhibition. This approach has been illustrated using the cell-permeable Nrf2 peptide, which is linked to fumarate through amide bonding to the lysine at the peptide's C-terminus. The peptide acts as a "pure Nrf2 activator," upregulating only the Nrf2 genetic program, as confirmed by transcriptomic analysis.

Another problem addressed in this work is associated with Nrf2 feedback regulation not only through Keap1, but also through transcriptional repressors such as Bach1, the target gene of Nrf2. To treat chronic conditions where sustained activation of the Nrf2 genetic program is necessary, the ideal Nrf2 activator must inhibit both Keap1 and Bach1. This approach is illustrated by the recently developed HMOX1 inducer from the group of benzothiazolyl-amino-benzimidazoles, HPPE, which exhibits both activities, e.g., Bach1 inhibition and Nrf2 activation, as confirmed by comparative transcriptomic analysis. The ongoing trials of HPPE and its variants have shown extremely promising results in oxidative stress scenarios [9].

CRediT authorship contribution statement

Dmitry M. Hushpulian: Writing – original draft, Visualization, Investigation, Data curation, Conceptualization. **Navneet Ammal Kaidery:** Writing – original draft, Visualization, Investigation, Data curation, Conceptualization. **Priyanka Soni:** Investigation, Data curation. **Andrey A. Poloznikov:** Writing – review & editing, Resources, Investigation. **Arpenik A. Zakhariants:** Investigation, Data curation. **Alexandra V. Razumovskaya:** Investigation, Data curation. **Mariia O. Silkina:** Investigation, Data curation. **Vladimir I. Tishkov:** Writing – review & editing. **Eliot H. Kazakov:** Investigation, Data curation. **Abraham M. Brown:** Writing – review & editing, Conceptualization. **Irina N. Gaisina:** Writing – review & editing, Investigation. **Young-Hoon Ahn:** Investigation, Data curation. **Sergey V. Kazakov:** Writing – review & editing. **Nancy Krucher:** Writing – review & editing, Data curation. **Sudarshana M. Sharma:** Writing – review & editing, Investigation, Conceptualization. **Bindu D. Paul:** Writing – review & editing, Resources. **Irina G. Gazaryan:** Writing – review & editing, Writing – original draft, Resources, Methodology, Conceptualization. **Sergey V. Nikulin:** Writing – review & editing, Writing – original draft, Supervision, Resources, Methodology, Investigation, Conceptualization. **Bobby Thomas:** Writing – review & editing, Writing – original draft, Supervision, Resources, Methodology, Funding acquisition, Formal analysis, Conceptualization.

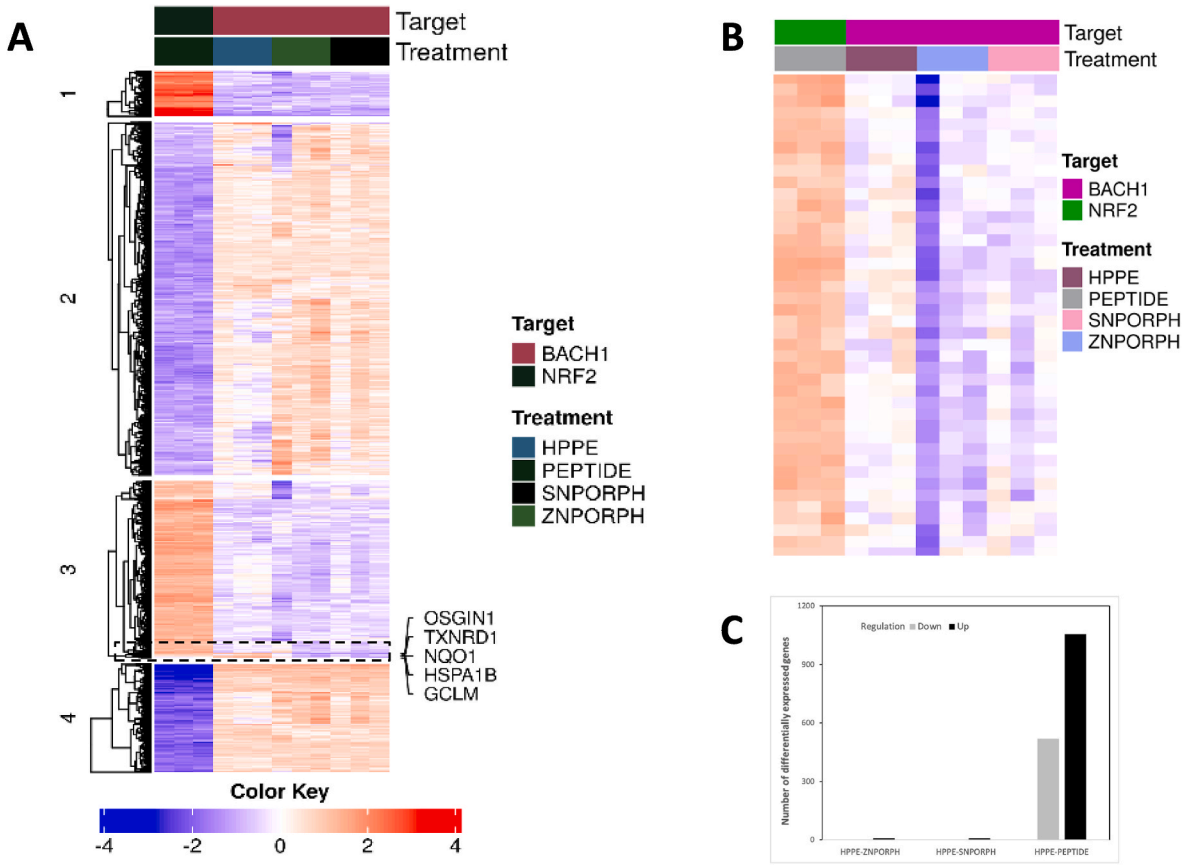

Fig. 7. Transcriptomic analysis differentiates gene signatures between Nrf2-peptide and Bach1 inhibitors. (A) K-means clustering of 2000 variable genes. (B) Magnified region from the dotted box in cluster 3 in (A), the annotation of the color bar is the same as in (A). (C) Differentially expressed genes (FDR $q < 0.1$, Log2FC $= 2$) between HPPE vs Nrf2 peptide, HPPE vs Zn protoporphyrin, and HPPE vs Sn-protoporphyrin.

Data availability

All data supporting the findings of this study are available within the article and its supplementary information. The RNA-seq data generated in this study are available in the Gene Expression Omnibus (GEO) repository (GSE271364 and GSE287793).

Funding

The work was supported by grants funded by the National Institutes of Health (R01AG077396, R01NS101967, and R01NS133688) and the Department of Defense (HT94252310443) to BT. This work was supported by the Basic Research Program at the National Research University Higher School of Economics to SN, AR, and MS for computer modeling and bioinformatic analysis. SMS is partially supported by the National Institutes of Health grant P01CA203653. BDP is supported by the American Heart Association and Paul Allen Foundation grant 19PABH134580006, R01AG071512, 1R21AG073684, the Solve-ME Foundation, and the Catalyst Award from Johns Hopkins University.

Declaration of competing interest

The authors declare that they have no known competing financial interests or personal relationships that could have appeared to influence the work reported in this paper.

Acknowledgements

The authors acknowledge Intelligenomica LLC for the genomic analysis support and graphics generation.

Appendix A. Supplementary data

Supplementary data to this article can be found online at https://doi.org/10.1016/j.redox.2025.103794.

References

[1] B. Harder, T. Jiang, T. Wu, S. Tao, M. Rojo de la Vega, W. Tian, E. Chapman, D. D. Zhang, Molecular mechanisms of Nrf2 regulation and how these influence chemical modulation for disease intervention, Biochem. Soc. Trans. 43 (2015) 680–686.
[2] O.H. Lee, A.K. Jain, V. Papusha, A.K. Jaiswal, 'An auto-regulatory loop between stress sensors INrf2 and Nrf2 controls their cellular abundance', J. Biol. Chem. 282 (2007) 36412–36420.
[3] H.K. Jyrkkanen, S. Kuosmanen, M. Heinaniemi, H. Laitinen, E. Kansanen, E. Mella-Aho, H. Leinonen, S. Yla-Herttuala, A.L. Levonen, Novel insights into the regulation of antioxidant-response-element-mediated gene expression by electrophiles: induction of the transcriptional repressor BACH1 by Nrf2, Biochem. J. 440 (2011) 167–174.
[4] A. Kopacz, D. Kloska, M. Targosz-Korecka, B. Zapotoczny, D. Cysewski, N. Personnic, E. Werner, K. Hajduk, A. Jozkowicz, A. Grochot-Przeczek, Keap1 governs ageing-induced protein aggregation in endothelial cells, Redox Biol. 34 (2020) 101572.
[5] T. Heurtaux, D.S. Bouvier, A. Benani, S. Helgueta Romero, K.B.M. Frauenknecht, M. Mittelbronn, L. Sinkkonen, Normal and pathological NRF2 signalling in the central nervous system, Antioxidants 11 (2022).
[6] J.L. Xiao, H.Y. Liu, C.C. Sun, C.F. Tang, Regulation of Keap1-Nrf2 signaling in health and diseases, Mol. Biol. Rep. 51 (2024) 809.
[7] N. Kubben, W. Zhang, L. Wang, T.C. Voss, J. Yang, J. Qu, G.H. Liu, T. Misteli, Repression of the antioxidant NRF2 pathway in premature aging, Cell 165 (2016) 1361–1374.
[8] A.T. Dinkova-Kostova, I.M. Copple, Advances and challenges in therapeutic targeting of NRF2, Trends Pharmacol. Sci. 44 (2023) 137–149.
[9] M. Ahuja, N. Ammal Kaidery, O.C. Attucks, E. McDade, D.M. Hushpulian, A. Gaisin, I. Gaisina, Y.H. Ahn, S. Nikulin, A. Poloznikov, I. Gazaryan, M. Yamamoto, M. Matsumoto, K. Igarashi, S.M. Sharma, B. Thomas, Bach1

derepression is neuroprotective in a mouse model of parkinson's disease, Proc. Natl. Acad. Sci. U. S. A. 118 (2021).
[10] N.A. Smirnova, R.E. Haskew-Layton, M. Basso, D.M. Hushpulian, J.B. Payappilly, R.E. Speer, Y.H. Ahn, I. Rakhman, P.A. Cole, J.T. Pinto, R.R. Ratan, I.G. Gazaryan, 'Development of Neh2-luciferase reporter and its application for high throughput screening and real-time monitoring of Nrf2 activators', Chem Biol 18 (2011) 752–765.
[11] T.D. Schmittgen, K.J. Livak, Analyzing real-time PCR data by the comparative C(T) method, Nat. Protoc. 3 (2008) 1101–1108.
[12] S. Parvez, Y. Fu, J. Li, M.J. Long, H.Y. Lin, D.K. Lee, G.S. Hu, Y. Aye, 'Substoichiometric hydroxynonenylation of a single protein recapitulates whole-cell-stimulated antioxidant response', J. Am. Chem. Soc. 137 (2015) 10–13.
[13] A. Lau, W. Tian, S.A. Whitman, D.D. Zhang, The predicted molecular weight of Nrf2: it is what it is not, Antioxid Redox Signal 18 (2013) 91–93.
[14] P. Ewels, M. Magnusson, S. Lundin, M. Kaller, 'MultiQC: summarize analysis results for multiple tools and samples in a single report', Bioinformatics 32 (2016) 3047–3048.
[15] S. Chen, Y. Zhou, Y. Chen, J. Gu, 'fastp: an ultra-fast all-in-one FASTQ preprocessor', Bioinformatics 34 (2018) i884–i890.
[16] A. Dobin, C.A. Davis, F. Schlesinger, J. Drenkow, C. Zaleski, S. Jha, P. Batut, M. Chaisson, T.R. Gingeras, STAR: ultrafast universal RNA-Seq aligner, Bioinformatics 29 (2013) 15–21.
[17] A. Frankish, M. Diekhans, A.M. Ferreira, R. Johnson, I. Jungreis, J. Loveland, J. M. Mudge, C. Sisu, J. Wright, J. Armstrong, I. Barnes, A. Berry, A. Bignell, S. Carbonell Sala, J. Chrast, F. Cunningham, T. Di Domenico, S. Donaldson, I. T. Fiddes, C. Garcia Giron, J.M. Gonzalez, T. Grego, M. Hardy, T. Hourlier, T. Hunt, O.G. Izuogu, J. Lagarde, F.J. Martin, L. Martinez, S. Mohanan, P. Muir, F.C. P. Navarro, A. Parker, B. Pei, F. Pozo, M. Ruffier, B.M. Schmitt, E. Stapleton, M. M. Suner, I. Sycheva, B. Uszczynska-Ratajczak, J. Xu, A. Yates, D. Zerbino, Y. Zhang, B. Aken, J.S. Choudhary, M. Gerstein, R. Guigo, T.J.P. Hubbard, M. Kellis, B. Paten, A. Reymond, M.L. Tress, P. Flicek, 'GENCODE reference annotation for the human and mouse genomes', Nucleic Acids Res. 47 (2019) D766–D773.
[18] Y. Liao, G.K. Smyth, W. Shi, The subread aligner: fast, accurate and scalable read mapping by seed-and-vote, Nucleic Acids Res. 41 (2013) e108.
[19] Y. Liao, G.K. Smyth, W. Shi, featureCounts: an efficient general purpose program for assigning sequence reads to genomic features, Bioinformatics 30 (2014) 923–930.
[20] Y. Zhang, G. Parmigiani, W.E. Johnson, ComBat-seq: batch effect adjustment for RNA-Seq count data, NAR Genom Bioinform 2 (2020) lqaa078.
[21] Z. Gu, D. Hubschmann, Make interactive complex heatmaps in R, Bioinformatics 38 (2022) 1460–1462.
[22] E.Y. Chen, C.M. Tan, Y. Kou, Q. Duan, Z. Wang, G.V. Meirelles, N.R. Clark, A. Ma'ayan, Enrichr: interactive and collaborative HTML5 gene list enrichment analysis tool, BMC Bioinf. 14 (2013) 128.
[23] P. Langfelder, S. Horvath, WGCNA: an R package for weighted correlation network analysis, BMC Bioinf. 9 (2008) 559.
[24] M. Ashburner, C.A. Ball, J.A. Blake, D. Botstein, H. Butler, J.M. Cherry, A.P. Davis, K. Dolinski, S.S. Dwight, J.T. Eppig, M.A. Harris, D.P. Hill, L. Issel-Tarver, A. Kasarskis, S. Lewis, J.C. Matese, J.E. Richardson, M. Ringwald, G.M. Rubin, G. Sherlock, 'Gene ontology: tool for the unification of biology. The Gene Ontology Consortium', Nat. Genet. 25 (2000) 25–29.
[25] P.D. Thomas, D. Ebert, A. Muruganujan, T. Mushayahama, L.P. Albou, H. Mi, PANTHER: making genome-scale phylogenetics accessible to all, Protein Sci. 31 (2022) 8–22.
[26] M.C. Lu, J.A. Ji, Y.L. Jiang, Z.Y. Chen, Z.W. Yuan, Q.D. You, Z.Y. Jiang, An inhibitor of the Keap1-Nrf2 protein-protein interaction protects NCM460 colonic cells and alleviates experimental colitis, Sci. Rep. 6 (2016) 26585.
[27] T. Plusa, Management of patients with chronic obstructive pulmonary disease (COPD) during COVID-19, Pol Merkur Lekarski 50 (2022) 262–263.
[28] T. Fukutomi, K. Takagi, T. Mizushima, N. Ohuchi, M. Yamamoto, 'Kinetic, thermodynamic, and structural characterizations of the association between Nrf2-DLGex degron and Keap1', Mol. Cell Biol. 34 (2014) 832–846.
[29] D.M. Hushpulian, N. Ammal Kaidery, M. Ahuja, A.A. Poloznikov, S.M. Sharma, I. G. Gazaryan, B. Thomas, Challenges and limitations of targeting the Keap1-Nrf2 pathway for neurotherapeutics: Bach1 De-Repression to the rescue, Front. Aging Neurosci. 13 (2021) 673205.
[30] T. Iso, T. Suzuki, L. Baird, M. Yamamoto, Absolute amounts and status of the Nrf2-Keap1-Cul3 complex within cells, Mol. Cell Biol. 36 (2016) 3100–3112.
[31] L. Hu, S. Magesh, L. Chen, L. Wang, T.A. Lewis, Y. Chen, C. Khodier, D. Inoyama, L. J. Beamer, T.J. Emge, J. Shen, J.E. Kerrigan, A.N. Kong, S. Dandapani, M. Palmer, S.L. Schreiber, B. Munoz, Discovery of a small-molecule inhibitor and cellular probe of Keap1-Nrf2 protein-protein interaction, Bioorg. Med. Chem. Lett. 23 (2013) 3039–3043.
[32] A.F. Winkel, C.K. Engel, D. Margerie, A. Kannt, H. Szillat, H. Glombik, C. Kallus, S. Ruf, S. Gussregen, J. Riedel, A.W. Herling, A. von Knethen, A. Weigert, B. Brune, D. Schmoll, Characterization of RA839, a noncovalent small molecule binder to Keap1 and selective activator of Nrf2 signaling, J. Biol. Chem. 290 (2015) 28446–28455.
[33] Y. Sun, L. Zheng, B. Yang, S. Ge, Q. Li, M. Zhang, S. Shen, Y. Ying, 'Design, synthesis and evaluation of novel small molecules acting as Keap1-Nrf2 protein-protein interaction inhibitors', J Enzyme Inhib Med Chem 37 (2022) 2575–2588.
[34] I.N. Gaisina, D.M. Hushpulian, A.M. Gaisin, E.H. Kazakov, N. Ammal Kaidery, M. Ahuja, A.A. Poloznikov, I.G. Gazaryan, G.R.J. Thatcher, B. Thomas, Identification of a potent Nrf2 displacement activator among aspirin-containing prodrugs, Neurochem. Int. 149 (2021) 105148.
[35] L. Jagannathan, S. Cuddapah, M. Costa, Oxidative stress under ambient and physiological oxygen tension in tissue culture, Curr Pharmacol Rep 2 (2016) 64–72.
[36] H.A. Edres, N.M. Taha, M.A. Lebda, M.S. Elfeky, The potential neuroprotective effect of allicin and melatonin in acrylamide-induced brain damage in rats, Environ. Sci. Pollut. Res. Int. 28 (2021) 58768–58780.
[37] R. Milo, What is the total number of protein molecules per cell volume? A call to rethink some published values, Bioessays 35 (2013) 1050–1055.
[38] L.T. Grinberg, U. Rueb, H. Heinsen, Brainstem: neglected locus in neurodegenerative diseases, Front. Neurol. 2 (2011) 42.
[39] S. Dutt, Y. Li, M. Mather, D.A. Nation, Initiative Alzheimer's Disease Neuroimaging, Brainstem substructures and cognition in prodromal alzheimer's disease, Brain Imaging Behav 15 (2021) 2572–2582.
[40] S. Vijayan, B. Singh, S. Ghosh, R. Stell, F.L. Mastaglia, Brainstem ventilatory dysfunction: a plausible mechanism for dyspnea in parkinson's disease? Mov. Disord. 35 (2020) 379–388.
[41] Y. Sun, J. Huang, Y. Chen, H. Shang, W. Zhang, J. Yu, L. He, C. Xing, C. Zhuang, Direct inhibition of Keap1-Nrf2 protein-protein interaction as a potential therapeutic strategy for alzheimer's disease, Bioorg. Chem. 103 (2020) 104172.
[42] I. Majkutewicz, Dimethyl fumarate: a review of preclinical efficacy in models of neurodegenerative diseases, Eur. J. Pharmacol. 926 (2022) 175025.
[43] Y. Sun, L. Xu, D. Zheng, J. Wang, G. Liu, Z. Mo, C. Liu, W. Zhang, J. Yu, C. Xing, L. He, C. Zhuang, A potent phosphodiester Keap1-Nrf2 protein-protein interaction inhibitor as the efficient treatment of alzheimer's disease, Redox Biol. 64 (2023) 102793.
[44] T. Pant, N. Uche, M. Juric, J. Zielonka, X. Bai, 'Regulation of immunomodulatory networks by Nrf2-activation in immune cells: redox control and therapeutic potential in inflammatory diseases', Redox Biol. 70 (2024) 103077.
[45] Y. Jung, S.E. Byeon, D.S. Yoo, Y.G. Lee, T. Yu, Y. Yang, J.H. Kim, E. Kim, D. Jeong, M.H. Rhee, E.S. Choung, S. Hong, J.Y. Cho, '8-(Tosylamino)quinoline inhibits macrophage-mediated inflammation by suppressing NF-kappaB signaling', Acta Pharmacol. Sin. 33 (2012) 1037–1046.
[46] C. Zhuang, S. Narayanapillai, W. Zhang, Y.Y. Sham, C. Xing, Rapid identification of Keap1-Nrf2 small-molecule inhibitors through structure-based virtual screening and hit-based substructure search, J. Med. Chem. 57 (2014) 1121–1126.
[47] M.C. Lu, H.L. Shao, T. Liu, Q.D. You, Z.Y. Jiang, Discovery of 2-oxy-2-phenylacetic acid substituted naphthalene sulfonamide derivatives as potent KEAP1-NRF2 protein-protein interaction inhibitors for inflammatory conditions, Eur. J. Med. Chem. 207 (2020) 112734.
[48] C.S. Jiang, C.L. Zhuang, K. Zhu, J. Zhang, L.A. Muehlmann, J.P. Figueiro Longo, R. B. Azevedo, W. Zhang, N. Meng, H. Zhang, Identification of a novel small-molecule Keap1-Nrf2 PPI inhibitor with cytoprotective effects on LPS-Induced cardiomyopathy, J Enzyme Inhib Med Chem 33 (2018) 833–841.
[49] R. Hancock, H.C. Bertrand, T. Tsujita, S. Naz, A. El-Bakry, J. Laoruchupong, J. D. Hayes, G. Wells, 'Peptide inhibitors of the Keap1-Nrf2 protein-protein interaction', Free Radic. Biol. Med. 52 (2012) 444–451.
[50] R. Steel, J. Cowan, E. Payerne, M.A. O'Connell, M. Searcey, 'Anti-inflammatory Effect of a Cell-Penetrating Peptide Targeting the Nrf2/Keap1 Interaction', ACS Med. Chem. Lett. 3 (2012) 407–410.
[51] K.P. Carrow, H.L. Hamilton, M.P. Hopps, Y. Li, B. Qiao, N.C. Payne, M. P. Thompson, X. Zhang, A. Magassa, M. Fattah, S. Agarwal, M.P. Vincent, M. Buyanova, P.A. Bertin, R. Mazitschek, M. Olvera de la Cruz, D.A. Johnson, J. A. Johnson, N.C. Gianneschi, Inhibiting the Keap1/Nrf2 protein-protein interaction with protein-like polymers, Adv Mater 36 (2024) e2311467.
[52] J.M. Mesfin, K.P. Carrow, A. Chen, M.P. Hopps, J.J. Holm, Q.P. Lyons, M. B. Nguyen, J.D. Hunter, A. Magassa, E.G. Wong, K. Reimold, S.N. Paleti, E. Gardner, M.P. Thompson, C.G. Luo, X. Zhang, K.L. Christman, N.C. Gianneschi, 'Protein-Like Polymers Targeting Keap1/Nrf2 as Therapeutics for Myocardial Infarction', Adv Mater (2025) e2417885.
[53] J. Tu, X. Zhang, Y. Zhu, Y. Dai, N. Li, F. Yang, Q. Zhang, D.W. Brann, R. Wang, 'Cell-Permeable Peptide Targeting the Nrf2-Keap1 Interaction: a Potential Novel Therapy for Global Cerebral Ischemia', J. Neurosci. 35 (2015) 14727–14739.
[54] M. Ahuja, N. Ammal Kaidery, L. Yang, N. Calingasan, N. Smirnova, A. Gaisin, I. N. Gaisina, I. Gazaryan, D.M. Hushpulian, I. Kaddour-Djebbar, W.B. Bollag, J. C. Morgan, R.R. Ratan, A.A. Starkov, M.F. Beal, B. Thomas, Distinct Nrf2 signaling mechanisms of fumaric acid esters and their role in neuroprotection against 1-Methyl-4-Phenyl-1,2,3,6-Tetrahydropyridine-Induced experimental parkinson's-like disease, J. Neurosci. 36 (2016) 6332–6351.
[55] S.H. Xiao, Y. Wang, X. Cao, Z. Su, Long non-coding RNA LUCAT1 inhibits myocardial oxidative stress and apoptosis after myocardial infarction via targeting microRNA-181a-5p, Bioengineered 12 (2021) 4546–4555.
[56] S. Ma, I.Y. Attarwala, X.Q. Xie, SQSTM1/p62: a potential target for neurodegenerative disease, ACS Chem. Neurosci. 10 (2019) 2094–2114.
[57] B. Shu, J. Jia, J. Zhang, V. Sethuraman, X. Yi, G. Zhong, DnaJ homolog subfamily A member1 (DnaJ1) is a newly discovered anti-apoptotic protein regulated by azadirachtin in Sf9 cells, BMC Genom. 19 (2018) 413.
[58] J. Simoes-Correia, D.I. Silva, S. Melo, J. Figueiredo, J. Caldeira, M.T. Pinto, H. Girao, P. Pereira, R. Seruca, DNAJB4 molecular chaperone distinguishes WT from mutant E-cadherin, determining their fate in vitro and in vivo, Hum. Mol. Genet. 23 (2014) 2094–2105.
[59] J.X. Lei, C.G. Cassone, C. Luebbert, Q.Y. Liu, A novel neuron-enriched protein SDIM1 is Down regulated in Alzheimer's brains and attenuates cell death induced by DNAJB4 over-expression in neuro-progenitor cells, Mol. Neurodegener. 6 (2011) 9.

[60] Y. Feng, M.Y. Jin, D.W. Liu, L. Wei, 'Proteasome subunit-alpha type-6 protein is post-transcriptionally repressed by the microRNA-4490 in diabetic nephropathy', Biosci. Rep. 38 (2018).
[61] H.D. Nguyen, W.K. Kim, G. Huong Vu, Molecular mechanisms implicated in protein changes in the alzheimer's disease human hippocampus, Mech. Ageing Dev. 219 (2024) 111930.
[62] J. Xie, Y. Zhang, B. Li, W. Xi, Y. Wang, L. Li, C. Liu, L. Shen, B. Han, Y. Kong, H. Yao, Z. Zhang, Inhibition of OGFOD1 by FG4592 confers neuroprotection by activating unfolded protein response and autophagy after ischemic stroke, J. Transl. Med. 22 (2024) 248.
[63] R.S. Singleton, P. Liu-Yi, F. Formenti, W. Ge, R. Sekirnik, R. Fischer, J. Adam, P. J. Pollard, A. Wolf, A. Thalhammer, C. Loenarz, E. Flashman, A. Yamamoto, M. L. Coleman, B.M. Kessler, P. Wappner, C.J. Schofield, P.J. Ratcliffe, M.E. Cockman, OGFOD1 catalyzes prolyl hydroxylation of RPS23 and is involved in translation control and stress granule formation, Proc. Natl. Acad. Sci. U. S. A. 111 (2014) 4031–4036.
[64] L. Chen, H. Wang, S. Vicini, R.W. Olsen, The gamma-aminobutyric acid type A (GABAA) receptor-associated protein (GABARAP) promotes GABAA receptor clustering and modulates the channel kinetics, Proc. Natl. Acad. Sci. U. S. A. 97 (2000) 11557–11562.
[65] X. Du, Z. Qi, J. Xu, M. Guo, X. Zhang, Z. Yu, X. Cao, J. Xia, 'Loss of GABARAPL1 confers ferroptosis resistance to cancer stem-like cells in hepatocellular carcinoma', Mol. Oncol. 16 (2022) 3703–3719.
[66] M. Puigdellivol, S. Milde, A. Vilalta, T.O.J. Cockram, D.H. Allendorf, J.Y. Lee, J. M. Dundee, K. Pampuscenko, V. Borutaite, H.N. Nuthall, J.H. Brelstaff, M. G. Spillantini, G.C. Brown, The microglial P2Y(6) receptor mediates neuronal loss and memory deficits in neurodegeneration, Cell Rep. 37 (2021) 110148.
[67] S. Anwar, V. Pons, S. Rivest, Microglia purinoceptor P2Y6: an emerging therapeutic target in CNS diseases, Cells 9 (2020).
[68] M. Le Vasseur, V.C. Chen, K. Huang, W.A. Vogl, C.C. Naus, Pannexin 2 localizes at ER-Mitochondria contact sites, Cancers (Basel) 11 (2019).
[69] D. Liao, G. Yang, Y. Yang, X. Tang, H. Huang, J. Shao, Q. Pan, Identification of pannexin 2 as a novel marker correlating with ferroptosis and malignant phenotypes of prostate cancer cells, OncoTargets Ther. 13 (2020) 4411–4421.
[70] H.R. Park, D. Azzara, E.D. Cohen, S.R. Boomhower, A.R. Diwadkar, B.E. Himes, M. A. O'Reilly, Q. Lu, Identification of novel NRF2-dependent genes as regulators of lead and arsenic toxicity in neural progenitor cells, J Hazard Mater 463 (2024) 132906.
[71] X. Chen, X. Wu, Y. Zhao, G. Wang, J. Feng, Q. Li, G. Qian, 'A novel binding protein of single immunoglobulin IL-1 receptor-related molecule: paralemmin-3', Biochem. Biophys. Res. Commun. 404 (2011) 1029–1033.
[72] G. Buccheri, D. Ferrigno, A. Curcio, F. Vola, E. Mattalia, MACC (methotrexate, doxorubicin, cyclophosphamide and lomustine) versus cis-platinum and etoposide in the treatment of advanced non-small cell lung cancer, Chemioterapia 5 (1986) 53–57.
[73] M. Patel, K.S. Taskar, M.J. Zamek-Gliszczynski, 'Importance of Hepatic Transporters in Clinical Disposition of Drugs and Their Metabolites', J. Clin. Pharmacol. 56 (Suppl 7) (2016) S23–S39.
[74] R. Alva, F. Moradi, P. Liang, J.A. Stuart, Culture of cancer cells at physiological oxygen levels affects gene expression in a cell-type specific manner, Biomolecules 12 (2022).
[75] A. Jyothidasan, S. Sunny, S. Murugesan, J.M. Quiles, A.K. Challa, B. Dalley, S. K. Cinghu, V. Nanda, N.S. Rajasekaran, 'Transgenic Expression of Nrf2 Induces a Pro-Reductive Stress and Adaptive Cardiac Remodeling in the Mouse', Genes 13 (2022).
[76] L. Gu, Y. Du, J. Chen, M.N. Hasan, Y.D. Clayton, D.J. Matye, J.E. Friedman, T. Li, Cullin 3 RING E3 ligase inactivation causes NRF2-dependent NADH reductive stress, hepatic lipodystrophy, and systemic insulin resistance, Proc. Natl. Acad. Sci. U. S. A. 121 (2024) e2320934121.
[77] H. Zhang, L. Zhou, K.J.A. Davies, H.J. Forman, 'Silencing Bach1 alters aging-related changes in the expression of Nrf2-regulated genes in primary human bronchial epithelial cells', Arch. Biochem. Biophys. 672 (2019) 108074.
[78] K. Ogawa, J. Sun, S. Taketani, O. Nakajima, C. Nishitani, S. Sassa, N. Hayashi, M. Yamamoto, S. Shibahara, H. Fujita, K. Igarashi, 'Heme mediates derepression of Maf recognition element through direct binding to transcription repressor Bach1', EMBO J. 20 (2001) 2835–2843.
[79] W. Hou, Y. Shan, J. Zheng, R.W. Lambrecht, S.E. Donohue, H.L. Bonkovsky, 'Zinc mesoporphyrin induces rapid and marked degradation of the transcription factor Bach1 and up-regulates HO-1', Biochim. Biophys. Acta 1779 (2008) 195–203.
[80] A. Abate, H. Zhao, R.J. Wong, D.K. Stevenson, The role of Bach1 in the induction of heme oxygenase by tin mesoporphyrin, Biochem. Biophys. Res. Commun. 354 (2007) 757–763.
[81] O.C. Attucks, K.J. Jasmer, M. Hannink, J. Kassis, Z. Zhong, S. Gupta, S.F. Victory, M. Guzel, D.R. Polisetti, R. Andrews, A.M. Mjalli, M.J. Kostura, 'Induction of heme oxygenase I (HMOX1) by HPP-4382: a novel modulator of Bach1 activity', PLoS One 9 (2014) e101044.
[82] R. Freeman, M.J. Bollong, HPPE activates NRF2 signaling by liberating heavy metal stores, Chembiochem (2024) e202400529.
[83] R.A. Zinovkin, N.D. Kondratenko, L.A. Zinovkina, Does Nrf2 play a role of a master regulator of mammalian aging? Biochemistry (Mosc) 87 (2022) 1465–1476.
[84] M. Diaz, C. Valdes-Baizabal, D.P. de Pablo, R. Marin, Age-dependent changes in Nrf2/Keap1 and target antioxidant protein expression correlate to lipoxidative adducts, and are modulated by dietary N-3 LCPUFA in the hippocampus of mice, Antioxidants 13 (2024).
[85] S. Davinelli, G. Scapagnini, F. Denaro, V. Calabrese, F. Benedetti, S. Krishnan, S. Curreli, J. Bryant, D. Zella, Altered expression pattern of Nrf2/HO-1 axis during accelerated-senescence in HIV-1 transgenic rat, Biogerontology 15 (2014) 449–461.
[86] H. Zhang, H. Liu, K.J. Davies, C. Sioutas, C.E. Finch, T.E. Morgan, H.J. Forman, Nrf2-regulated phase II enzymes are induced by chronic ambient nanoparticle exposure in young mice with age-related impairments, Free Radic. Biol. Med. 52 (2012) 2038–2046.
[87] V. Dias, E. Junn, M.M. Mouradian, The role of oxidative stress in parkinson's disease, J. Parkinsons Dis. 3 (2013) 461–491.
[88] S.A. Aleksander, J. Balhoff, S. Carbon, J.M. Cherry, H.J. Drabkin, D. Ebert, M. Feuermann, P. Gaudet, N.L. Harris, D.P. Hill, R. Lee, H. Mi, S. Moxon, C. J. Mungall, A. Muruganugan, T. Mushayahama, P.W. Sternberg, P.D. Thomas, K. Van Auken, J. Ramsey, D.A. Siegele, R.L. Chisholm, P. Fey, M.C. Aspromonte, M. V. Nugnes, F. Quaglia, S. Tosatto, M. Giglio, S. Nadendla, G. Antonazzo, H. Attrill, G. Dos Santos, S. Marygold, V. Strelets, C.J. Tabone, J. Thurmond, P. Zhou, S. H. Ahmed, P. Asanitthong, D. Luna Buitrago, M.N. Erdol, M.C. Gage, M. Ali Kadhum, K.Y.C. Li, M. Long, A. Michalak, A. Pesala, A. Pritazahra, S.C. C. Saverimuttu, R. Su, K.E. Thurlow, R.C. Lovering, C. Logie, S. Oliferenko, J. Blake, K. Christie, L. Corbani, M.E. Dolan, H.J. Drabkin, D.P. Hill, L. Ni, D. Sitnikov, C. Smith, A. Cuzick, J. Seager, L. Cooper, J. Elser, P. Jaiswal, P. Gupta, P. Jaiswal, S. Naithani, M. Lera-Ramirez, K. Rutherford, V. Wood, J.L. De Pons, M. R. Dwinell, G.T. Hayman, M.L. Kaldunski, A.E. Kwitek, S.J.F. Laulederkind, M. A. Tutaj, M. Vedi, S.J. Wang, P. D'Eustachio, L. Aimo, K. Axelsen, A. Bridge, N. Hyka-Nouspikel, A. Morgat, S.A. Aleksander, J.M. Cherry, S.R. Engel, K. Karra, S.R. Miyasato, R.S. Nash, M.S. Skrzypek, S. Weng, E.D. Wong, E. Bakker, T. Z. Berardini, L. Reiser, A. Auchincloss, K. Axelsen, G. Argoud-Puy, M.C. Blatter, E. Boutet, L. Breuza, A. Bridge, C. Casals-Casas, E. Coudert, A. Estreicher, M. Livia Famiglietti, M. Feuermann, A. Gos, N. Gruaz-Gumowski, C. Hulo, N. Hyka-Nouspikel, F. Jungo, P. Le Mercier, D. Lieberherr, P. Masson, A. Morgat, I. Pedruzzi, L. Pourcel, S. Poux, C. Rivoire, S. Sundaram, A. Bateman, E. Bowler-Barnett, A. Jee H. Bye, P. Denny, A. Ignatchenko, R. Ishtiaq, A. Lock, Y. Lussi, M. Magrane, M.J. Martin, S. Orchard, P. Raposo, E. Speretta, N. Tyagi, K. Warner, R. Zaru, A.D. Diehl, R. Lee, J. Chan, S. Diamantakis, D. Raciti, M. Zarowiecki, M. Fisher, C. James-Zorn, V. Ponferrada, A. Zorn, S. Ramachandran, L. Ruzicka, M. Westerfield, Gene Ontology, Consortium, 'The Gene Ontology knowledgebase in 2023', Genetics 224 (2023). PMID: 36866529.
[89] A.Y. Khristichenko, A.A. Poloznikov, D.M. Hushpulian, N.A. Smirnova, A. A. Zakhariants, S.V. Kazakov, V.I. Tishkov, I.G. Gazaryan, Quantitative analysis of cell-based luciferase fusion reporters, Mosc. Univ. Chem. Bull. 74 (2019) 180–185.